BOUNDARY LAYER SOLUTIONS IN THE GIERER-MEINHARDT SYSTEM WITH INHOMOGENEOUS BOUNDARY CONDITIONS

DANIEL GOMEZ, LINFENG MEI, JUNCHENG WEI

Abstract. The use of inhomogeneous boundary conditions has become increasingly important in the study of pattern forming reaction diffusion systems. Such inhomogeneities can be used to describe, for example, the interaction between an individual cell with its environment. In this paper we consider arbitrary mixed inhomogeneous boundary conditions for the activator in the singularly perturbed Gierer-Meinhardt system. By using formal asymptotics we derive an algebraic system and nonlocal eigenvalue problem respectively describing the structure and linear stability of multi-spike solutions in the case of a one-dimensional domain, thereby extending previous results obtained in the case of inhomogeneous Neumann boundary conditions by Gomez et. al. (J Nonlinear Sci 31, 37, 2021). We also rigorously prove partial stability results and provide detailed stability thresholds for two examples consisting of one- and two-spike solutions. In higher dimensions we restrict our attention to the shadow limit in which the inhibitor is well-mixed and for which we rigorously establish both the existence and stability of a boundary layer solution. In both the one- and higher-dimensional cases we find that when the boundary conditions are symmetric then a symmetric solution is stable only when the magnitude of the inhomogeneity exceeds some threshold. Below this threshold we demonstrate that a stable asymmetric two spike solution emerges in the case of a one-dimensional domain, while in the case of a two-dimensional domain we show numerical simulations illustrating the formation of a near-boundary spike.

1. Introduction

Initiated by Alan M. Turing's original insights into the role of diffusion and reaction-kinetics in the emergence of spatial patterns [23], reaction-diffusion systems have become a staple in studies of pattern formation. In such systems a change in the diffusivities of its constituents or other model parameters can lead to a Turing, or diffusion-driven, instability in which a spatially homogeneous steady state is driven out of equilibrium into a spatially patterned state. This provides an attractive mechanism for symmetry breaking not only in morphogenesis during early development, the context in which Turing's original ideas were developed, but also more broadly in the emergence of self-organization in complex systems.

While studies of pattern-forming reaction-diffusion systems typically assume the systems to be isolated, an assumption reflected by the common choice of homogeneous Neumann boundary conditions (BCs), the importance of different choices of boundary conditions has previously been highlighted [2]. More recently it has been shown that the specific introduction of inhomogeneous boundary conditions can lead to the formation of patterns that are isolated away from the boundary and may be more robust to perturbations in the initial conditions [14]. Moreover, studies of pattern formation in reaction-diffusion systems incorporating bulk-surface coupling [15, 21, 10, 16, 9, 5] and stratified domains [13] have highlighted the necessity of inhomogeneous boundary conditions for the bulk problem in models of intracellular pattern formation. In the context of singularly perturbed reaction-diffusion systems there is a small but growing body of literature detailing the effects of different boundary conditions on localized solutions. Such studies have investigated the effects of homogeneous mixed, or Robin, boundary conditions for the slowly diffusing activator in the Gierer-Meinhardt (GM) model [1, 17], as well as inhomogeneous mixed boundary conditions

Key words and phrases. singular perturbation, matched asymptotic expansions, Gierer-Meinhardt system, nonlocal eigenvalue problem (NLEP), pattern formation, boundary conditions.

for the faster diffusing substrate in the two-dimensional Brusselator model [24]. More recently, it was found that an inhomogeneous Neumann boundary condition for the slowly diffusing activator in the one-dimensional GM model leads to the formation of stable asymmetric boundary layer type solutions [7]. In this paper we extend the results found in [7] by studying the structure and stability of boundary layer solutions to the one-dimensional singularly perturbed GM model with inhomogeneous mixed boundary conditions, which includes as a special case both inhomogeneous Neumann and Dirichlet boundary conditions. In addition we consider the structure and stability of boundary layer solutions in higher dimensional domains with the caveat that the inhibitor diffusivity is infinitely large, i.e. in the so-called *shadow limit*.

In the singularly perturbed GM model the concentrations of an activator and inhibitor, U and V respectively, are determined by the system of equations

$$U_t = \varepsilon^2 \Delta U - U + \frac{U^2}{V}, \quad \tau V_t = D\Delta V - V + \frac{1}{\varepsilon}U^2, \qquad x \in \Omega, \tag{1.1a}$$

$$\frac{\partial V}{\partial \nu} = 0, \qquad \begin{cases} \varepsilon \frac{\partial U}{\partial \nu} + \kappa U = A, & x \in \partial\Omega \quad \text{(mixed BCs)}, \\ U = A, & x \in \partial\Omega \quad \text{(Dirichlet BCs)}. \end{cases} \tag{1.1b}$$

where $\Omega \subset \mathbb{R}^d$ $(d \geq 1)$ is a bounded domain, $\partial/\partial\nu$ denotes the derivative in the direction of the outward normal, and where $\varepsilon \ll 1$ is an asymptotically small parameter while $\kappa = \mathcal{O}(1)$ and $A = \mathcal{O}(1)$. Note that the Dirichlet BCs can be formally obtained from the mixed BCs by replacing A with κA and taking the limit $\kappa \to \infty$. Originally introduced in 1972 [4] as a model of pattern formation driven by short-range activation and long-range inhibition, the GM model (1.1) has since become a prototypical model for the formal and rigorous study of localized solutions [30]. Specifically, both the structure and dynamics of multi-spike quasi-equilibrium solutions to the singularly perturbed GM model in one-, and three-dimensional domains have been obtained using formal asymptotic methods in [11, 25, 26, 6]. Extensive rigorous existence and stability results have likewise been obtained when $D \to \infty$ [8, 12, 27] as well as for finite values of D [3, 22, 29, 28]. The particular scaling of the GM model used in (1.1) is chosen in such a way that steady-state boundary solutions concentrating in an $\mathcal{O}(\varepsilon)$ neighbourhood of the $(d-1)$-dimensional boundary $\partial\Omega$ are $\mathcal{O}(1)$ in magnitude as can readily be seen by integrating both the first and second equations in (1.1a) and using the divergence theorem.

In the first part of this paper we restrict our attention to the case $d = 1$ for which our results can be seen as a direct generalization of those obtain in [7]. Specifically in §2.1 we use the method of matched asymptotic expansion to construct an asymptotic approximation to a multi-spike solution. In §2.2 we very briefly outline the derivation of the nonlocal eigenvalue problem (NLEP) governing the linear stability of such multi-spike solutions and in §2.3 we use a continuation argument to rigorously establish partial stability results for a single boundary-bound spike solution. Finally in §2.4 and §2.5 we consider two examples which illustrate in detail the behaviour of a solution consisting of a single boundary-bound spike, as well as that of two boundary-bound spikes. In the second part of the paper we consider the formation of analogous boundary-layer solutions in higher dimensions when $D \to \infty$ by rigorously establishing their existence in §3.1 and their stability in §3.2. In §3.3 we perform numerical simulations to illustrate the stability properties of the boundary layer solution as well as to probe their long time dynamics beyond the onset of instabilities.

2. Multi-Spike Solutions in a One-Dimensional Domain

In a one-dimensional domain given by the interval $-1 < x < 1$ the singularly perturbed GM model (1.1) takes the form

$$u_t = \varepsilon^2 u_{xx} - u + v^{-1}u^2, \qquad \tau v_t = Dv_{xx} - v + \varepsilon^{-1}u^2, \qquad -1 < x < 1, \quad t > 0, \tag{2.1a}$$

with mixed

$$\pm\,\varepsilon u_x + \kappa u = A_\pm, \quad v_x = 0, \qquad x = \pm 1. \tag{2.1b}$$

or Dirichlet boundary conditions (BCs)

$$u = A_\pm, \qquad v_x = 0, \quad v_x = 0, \qquad x = \pm 1. \tag{2.1c}$$

The study of multi-spike solutions in the case of homogeneous mixed BCs were previously considered in [17] while inhomogeneous Neumann BCs (i.e. with $\kappa = 0$) with $A_\pm > 0$ were considered in [7]. Note that by letting $A_\pm = \kappa \bar{A}_\pm$ and taking the limit $\kappa \to \infty$ we can formally obtain the Dirichlet BCs (2.1c) from the mixed BCs (2.1). In the next section we will use the method of matched asymptotic expansions to reduce the problem of constructing multi-spike solutions of (2.1) to that of solving a system of algebraic equations for the spike *heights* and locations. This method has been successfully used in many other studies to construct multi-spike solutions and study their liner stability (see for example [11, 25]) and we therefore keep our presentation brief, providing only those details most pertinent to this paper.

2.1. **Multi-Spike Quasi-Equilibrium Solutions.** In order for us to use the method of matched asymptotic expansions to construct an $N+2$ multi-spike solution consisting of N spikes concentrating at $-1 < x_1 < ... < x_N < 1$ and two spikes concentrating at the boundaries $x = \pm 1$ we must assume that the spike locations are well separated in the sense that $|x_1+1|, |x_N-1|, |x_{i+1}-x_i| = \mathcal{O}(1)$ for all $i = 1, ..., N-1$. In this case the interaction between individual spikes is mediated by the faster diffusing inhibitor. Proceeding as in [7] an $N+2$ spike quasi-equilibrium solution can be constructed in terms of the homoclinic solution w_c satisfying

$$w_c'' - w_c + w_c^2 = 0, \quad -\infty < y < \infty; \qquad w_c'(0) = 0, \quad w_c \to 0, \quad |y| \to \infty, \tag{2.2}$$

and the Neumann Green's function $G_\mu(x,\zeta)$ satisfying

$$D\partial_x^2 G_\mu - (1+\mu)G_\mu = -\delta(x-\zeta), \quad -1 < x, \zeta < 1; \quad D\partial_x G_\mu(x,\zeta) = 0, \qquad x = \pm 1, \tag{2.3}$$

both of which are respectively given by

$$w_c(y) = \frac{3}{2}\mathrm{sech}^2\big(\tfrac{1}{2}y\big), \quad G_\mu(x,\zeta) = \frac{\cosh\sqrt{\frac{1+\mu}{D}}(2-|x-\zeta|) + \cosh\sqrt{\frac{1+\mu}{D}}(x+\zeta)}{2\sqrt{(1+\mu)D}\sinh 2\sqrt{\frac{1+\mu}{D}}}. \tag{2.4}$$

In particular (see [7] for details) we find that as $\varepsilon \to 0^+$ an asymptotic approximation for such a multi-spike solution is given by

$$u \sim \sum_{i=1}^N \xi_i w_c\big(\tfrac{x-x_i}{\varepsilon}\big) + \sum_{\pm} \xi_\pm w_c\big(\tfrac{1\mp x}{\varepsilon} + y_\pm\big), \quad v \sim 6\sum_{i=1}^N \xi_i^2 G_0(x,x_i) + \sum_{\pm}\eta(y_\pm)\xi_\pm^2 G_0(x,\pm 1), \tag{2.5}$$

where

$$\eta(y_0) \equiv \int_0^\infty w_c(y+y_0)^2 dy = 6\frac{e^{-2y_0}(3+e^{-y_0})}{(1+e^{-y_0})^3}, \tag{2.6}$$

and where the boundary spike *shift* parameters, y_- and y_+, are chosen to satisfy

$$-w_c'(y_\pm) + \kappa w_c(y_\pm) = \xi_\pm^{-1} A_\pm, \tag{2.7}$$

while the spike *heights*, $\xi_\pm$ and $\xi_1, ..., \xi_N$, are found by solving the nonlinear algebraic system

$$\boldsymbol{B} = 0, \qquad \text{where} \quad \boldsymbol{B} \equiv \boldsymbol{\xi} - \mathcal{G}_0 \mathcal{N} \boldsymbol{\xi}^2, \tag{2.8}$$

where

$$\boldsymbol{\xi} \equiv (\xi_-, \xi_1, \cdots, \xi_N, \xi_+)^T, \quad \mathcal{N} \equiv \mathrm{diag}(\eta(y_-), 6, \cdots, 6, \eta(y_+)) \tag{2.9}$$

and

$$\mathcal{G}_0 \equiv \begin{pmatrix} G_0(-1,-1) & G_0(-1,x_1) & \cdots & G_0(-1,x_N) & G_0(-1,1) \\ G_0(x_1,-1) & G_0(x_1,x_1) & \cdots & G_0(x_1,x_N) & G_0(x_1,1) \\ \vdots & \vdots & \ddots & \vdots & \vdots \\ G_0(x_N,-1) & G_0(x_N,x_1) & \cdots & G_0(x_N,x_N) & G_0(x_N,1) \\ G_0(1,-1) & G_0(1,x_1) & \cdots & G_0(1,x_N) & G_0(1,1) \end{pmatrix}. \tag{2.10}$$

Without additional constraints on the interior spike locations the interior spikes undergo slow drift dynamics over an $\mathcal{O}(\varepsilon^{-2})$ timescale. Although we will not be interested in interior spike dynamics in this paper we remark that by letting $x_i = x_i(\varepsilon^2 t)$ a higher order solvability condition (see for example §5 in [11] for details) yields the system of ODEs

$$\frac{1}{\varepsilon^2}\frac{dx_i}{dt} = -6\xi_i \big\langle \partial_x G_0(x,x_i)\big\rangle_{x=x_i} - \frac{2}{\xi_i}\left(6\sum_{j\neq i}\xi_j^2 \partial_x G_0(x_i,x_j) + \sum_{\pm}\eta(y_\pm)\xi_\pm^2\partial_x G_0(x_i,\pm 1)\right), \tag{2.11}$$

for each $i = 1,...,N$ which is to be solved in conjunction with the algebraic system (2.8) and where

$$\langle f(x)\rangle_{x=x_0} \equiv \lim_{x\to x_0^+} f(x) + \lim_{x\to x_0^-} f(x). \tag{2.12}$$

Thus, while (2.8) yields the spike heights for any spike configuration, only those solutions for which the locations are steady states of (2.11) will be stationary on an $\mathcal{O}(\varepsilon^{-2})$ timescale.

2.1.1. *Gluing Method.* An alternative method for constructing multi-spike equilibrium solutions, previously used to construct asymmetric multi-spike solutions in [25] and recently extended to the case of inhomogeneous Neumann BCs in [7], first involves partitioning the interval $-1 < x < 1$ into $N+2$ mutually disjoint sub-intervals given by

$$I_- = (-1,-1+l_-), \quad I_+ = (1-l_+,1), \quad I_i = [x_i - l_i, x_i + l_i) \quad (i = 1,...,N),$$

where $x_i = -1+l_-+2\sum_{j=1}^{i-1} l_j + l_i$ and the $N+2$ positive parameters $l_\pm, l_1, ..., l_N$ are to be determined. The multi-spike equilibrium solution is then asymptotically approximated by the piecewise functions (see [7] for details)

$$u_e(x) \sim \begin{cases} u_0(1\mp x; l_\pm, A_\pm, \kappa), & x\in I_\pm \\ u_0(|x-x_i|; l_i, 0, 0), & x\in I_i \end{cases}, \quad v_e(x) \sim \begin{cases} v_0(1\mp x; l_\pm, A_\pm, \kappa), & x\in I_\pm \\ v_0(|x-x_i|; l_i, 0, 0), & x\in I_i \end{cases}, \tag{2.13}$$

in terms of

$$u_0(x;l,A,\kappa) \equiv \xi_0 w_c(\varepsilon^{-1}x + y_0), \quad v_0(x;l,A,\kappa) \equiv \xi_0 \cosh\big(\tfrac{l-x}{\sqrt{D}}\big)\operatorname{sech}\big(\tfrac{l}{\sqrt{D}}\big) \tag{2.14a}$$

where y_0 and ξ_0 are functions of l, A, and κ given by

$$\xi_0 = \frac{\sqrt{D}}{\eta(y_0)}\tanh\left(\frac{l}{\sqrt{D}}\right), \quad y_0 = \begin{cases} \log\big(\frac{1-\kappa+3q+\sqrt{(1-\kappa+3q)^2+4(1+\kappa)q}}{2(1+\kappa)}\big), & \text{for } 0\le\kappa<\infty, \\ \log\big(\frac{3q-1+\sqrt{(3q-1)^2+4q}}{2}\big), & \text{for Dirichlet BCs,} \end{cases} \tag{2.14b}$$

(2.14c)

and where

$$q \equiv \frac{A/\sqrt{D}}{\tanh(l/\sqrt{D})}. \tag{2.14d}$$

The parameters $l_-, l_1, ..., l_N, l_+$ are then chosen in such a way that the resulting piecewise function is continuous in $-1 < x < 1$ from which we deduce the constraints

$$l_- + 2l_1 + \cdots 2l_N + l_+ = 2, \tag{2.15a}$$

$$v_0(l_-;l_-,A_-,\kappa) = v_0(l_1;l_1,0,0) = \cdots = v_0(l_N;l_N,0,0) = v_0(l_+;l_+,A_+,\kappa). \tag{2.15b}$$

To ensure the argument of the logarithm in (2.14b) is real and nonnegative it can be shown that we require that $q \geq q_{\min}(\kappa)$ where

$$q_{\min}(\kappa) \equiv \begin{cases} \frac{\kappa-5+\sqrt{(\kappa-5)^2-9(\kappa-1)^2}}{9}, & \text{for } 0 \leq \kappa < 1, \\ 0, & \text{for } \kappa \geq 1 \text{ and Dirichlet BCs.} \end{cases} \tag{2.16}$$

This in turn implies the lower bounds $y_0 > y_{\min}(\kappa)$ where

$$y_{\min}(\kappa) \equiv \begin{cases} \log\left(\frac{1-\kappa+3q_{\min}(\kappa)}{2(1+\kappa)}\right), & \text{for } 0 \leq \kappa < 1, \\ -\infty, & \text{for } \kappa \geq 1 \text{ and Dirichlet BCs,} \end{cases} \tag{2.17}$$

as well as $A > \sqrt{D} q_{min}(\kappa) \tanh(l/\sqrt{D})$ which implies in particular that A must be strictly positive for $\kappa > 1$ as well as Dirichlet BCs, though it may be negative for $0 \leq \kappa < 1$.

As previously identified in [17, 7] the shift parameter plays an important role in the linear stability of a single spike solution. Using (2.4) it is easy to see that when $0 \leq \kappa < 1$ the function $-w_c'(y_0)+\kappa w_c(y_0)$ has exactly two critical points at which it attains a global minimum and maximum and which are respectively given by

$$\tilde{y_c}(\kappa) \equiv \log\left(\frac{3-\kappa-\sqrt{\kappa^2+3}}{3+\kappa+\sqrt{\kappa^2+3}}\right), \qquad y_c(\kappa) \equiv \log\left(\frac{3-\kappa+\sqrt{\kappa^2+3}}{3+\kappa-\sqrt{\kappa^2+3}}\right). \tag{2.18}$$

As $\kappa \to 1^-$ it is easy to see that $\tilde{y}_c \to -\infty$ and in particular for $\kappa \geq 1$ there is only one critical point and it is a global maximum at $y_0 = y_c(\kappa)$. Moreover for Dirichlet BCs there is a unique global maximum at $y_0 = y_c(+\infty) = 0$. It can further be shown that $\tilde{y}_c < y_{\min}$ for $0 \leq \kappa < 1$. The value $y_c(\kappa)$ plays an important role in the linear stability of single spike solutions and we use it to distinguish between two types of spike solutions:

(1) *large-shift* solutions for which $y_0 > y_c(\kappa)$ and hence $-w_c''(y_0) + \kappa w_c'(y_0) < 0$ (or $y_0 > 0$ and $w_c'(y_0) < 0$ for Dirichlet BCs), and
(2) *small-shift* solutions for which $y_{\min}(\kappa) < y_0 < y_c(\kappa)$ and hence $-w_c''(y_0) + \kappa w_c'(y_0) > 0$ (or $y_0 < 0$ and $w_c'(y_0) > 0$ for Dirichlet BCs).

We plot both $y_{\min}$ and y_c (together with other critical values) in Figure 1a. In a sense made more precise in §2.3, a large-shift solution is more stable than a small shift solution. Moreover the stability of large shift solutions extends to higher dimensional boundary layer solutions as is rigorously established in §3 below.

2.2. **Linear Stability.** To calculate the stability of the equilibrium multi-spike solutions constructed above we let $u = u_e + e^{\lambda t}\phi$ and $v = v_e + e^{\lambda t}\psi$ where $u = u_e$ and $v = v_e$ is constructed using either of the methods outlined above. It can then be shown using the method of matched asymptotic expansions that the eigenvalues $\lambda = \mathcal{O}(1)$ are determined by the system of nonlocal eigenvalue problems (see §3 in [7] for details)

$$\mathscr{L}_{y_i}\phi_i - 2w_c(y+y_i)^2 \sum_{j=\pm,1}^{N} \hat{\xi}_j G_{\tau\lambda}(x_i,x_j) \frac{\int_0^\infty w_c(y+y_j)\phi_j(y)\,dy}{\eta(y_j)} = \lambda\phi_i, \tag{2.19}$$

for $i = \pm, 1, ..., N$ where $G_{\tau\lambda}(x_i, x_j)$ is the Green's function defined in (2.4) and where

$$\hat{\xi}_\pm = \eta(y_\pm)\xi_\pm, \qquad \hat{\xi}_i = 12\xi_i, \quad \mathscr{L}_{y_i}\phi \equiv \phi'' - \phi + 2w_c(y+y_i)\phi, \qquad (i = 1, ..., N), \tag{2.20}$$

and we set $y_1 = ... = y_N = 0$ (i.e. no shift for the interior spikes). By decomposing each $\phi_1, ..., \phi_N$ into even and odd components in y it can be shown that a nontrivial odd component always yields $\lambda \leq 0$. As a consequence, to determine conditions under which unstable eigenvalues arise it suffices

to restrict our attention to the case where each $\phi_1, ..., \phi_N$ is even in y. In particular the problem for each $\phi_\pm, \phi_1, .., \phi_N$ can be posed on the half interval $0 < y < \infty$ with the BCs

$$\begin{cases} -\phi_\pm' + \kappa\phi_\pm = 0 \quad \text{or} \quad \phi_\pm = 0, \quad \phi_1' = ... = \phi_N' = 0, & \text{at } y = 0, \\ \phi_\pm, \phi_1, ..., \phi_N \longrightarrow 0, & \text{as } y \to +\infty. \end{cases} \tag{2.21}$$

In the next subsection we rigorously establish some stability properties of th NLEP (2.19) in the case of a single spike concentrating at $x = -1$ while in §2.4-2.5 we directly calculate stability thresholds from (2.19) for a one- and a two-spike solution.

2.3. **Rigorous Stability Results.** In this section we rigorously prove partial stability and instability results for the NLEP

$$\mathscr{L}_{y_0}\phi - \mu\frac{\int_0^\infty w(y)\phi(y)dy}{\int_0^\infty w(y)^2dy}w^2 = \lambda\phi, \quad 0 < y < \infty, \tag{2.22}$$

with $\phi \to 0$ as $y \to +\infty$ and either mixed or Dirichlet BCs at $y = 0$ respectively given by

$$-\phi'(0) + \kappa\phi(0) = 0, \qquad \phi(0) = 0, \tag{2.23}$$

where μ, κ, and y_0 are real constants and where

$$\mathscr{L}_{y_0}\phi \equiv \phi'' - \phi + 2w\phi, \qquad w(y) \equiv w_c(y + y_0), \tag{2.24}$$

and $w_c(y)$ is the homoclinic given in (2.4). The proofs in the remainder of this subsection closely follow those used in [7] for the $\kappa = 0$ and $A \geq 0$ case. The remainder of this subsection is organized as follows. First we establish some key spectral properties of the linearized operator $\mathscr{L}_{y_0}$. We then establish partial stability results for small shift solutions in Theorem 2.1 and for large shift solutions in Theorem 2.2. Finally, we conclude by proving partial instability results for small-shift solutions.

Lemma 2.1. *Let $\Lambda_0 \geq \Lambda_1$ be the two largest eigenvalues and Φ_0 and Φ_1 the corresponding eigenfunctions of $\mathscr{L}_{y_0}$ with mixed or Dirichlet BCs (2.23). Then for all $\kappa \geq 0$ (with $\kappa = +\infty$ for Dirichlet BCs) we have:*

(i) Φ_0 is of one sign.
(ii) If $y_{min}(\kappa) < y_0 < y_c(\kappa)$ then $\Lambda_0 > 0$.
(iii) If $y_0 > y_c(\kappa)$ then $\Lambda_0 < 0$.
(iv) If $y_0 = y_c(\kappa)$ then $\Lambda = 0$ and $\Phi_0 = w'$.
(v) $\Lambda_1 < 0$ for all $y_0 > y_{min}(\kappa)$.

Proof. We prove each item in the case of mixed BCs and remark that the same arguments hold for Dirichlet BCs by taking the limit $\kappa \to \infty$. From the variational characterization of the principal eigenvalue

$$-\Lambda_0 = \inf_{\Phi \in H^1([0,\infty))} \frac{\int_0^\infty \left[|\Phi'(y)|^2 + \Phi(y)^2 - 2w(y)\Phi(y)^2\right]dy + \kappa\Phi(0)^2}{\int_0^\infty \Phi(y)^2dy}, \tag{2.25}$$

we deduce that the principal eigenfunction can be achieved by a positive function (otherwise replacing it with its absolute value) which proves (i). To prove (ii) we use the test function $\Phi(y) = w'(y)$ in (2.25) and integrate by parts to get

$$-\Lambda_0 \leq \frac{w'(0)[-w''(0) + \kappa w'(0)]}{\int_0^\infty w'(y)^2dy}, \tag{2.26}$$

for which we note that the right hand side is strictly negative if $0 < y_0 < y_c$. On the other hand, if $y_{\min} < y_0 < 0$ we multiply $\mathscr{L}_{y_0}\Phi_0 = \Lambda_0\Phi_0$ by $w'(y)$ and integrate from $-y_0$ to ∞ to get

$$\Lambda_0 = \frac{\Phi_0(-y_0)w_c''(0)}{\int_{-y_0}^\infty \Phi_0(y)w'(y)dy} > 0, \tag{2.27}$$

where we have used that $w_c''(0) < 0$ and $w'(y) = w_c'(y + y_0) < 0$ for all $y > -y_0$. If instead $y_0 > y_c$ then we again multiply $\mathscr{L}_{y_0}\Phi_0 = \Lambda\Phi_0$ by $w'(y)$ but this time integrate from 0 to ∞ to get

$$\Lambda_0 = -\frac{\Phi_0(0)[-w''(0) + \kappa w'(0)]}{\int_0^\infty \Phi_0(y)w'(y)dy} < 0, \tag{2.28}$$

which proves (iii). The proof of (iv) is a direct calculation.

Finally, we prove (v) by considering the cases $y_0 \geq 0$ and $y_{\min} < y_0 < 0$ separately. When $y_0 \geq 0$ the proof is identical to the case $\kappa = 0$ which was proved in Lemma 4.2 of [7]. When $y_0 < 0$ then w' is no longer of one sign and the argument from $\kappa = 0$ no longer holds. We begin by assuming that $\Lambda_1 \geq 0$. First, since Φ_0 is of one sign Φ_1 must change signs at least once. Then since $w'(y) < 0$ for all $y > -y_0$ the same argument from Lemma 4.2 [7] implies that Φ_1 can't have any zeros in $(-y_0, +\infty)$. Therefore we may assume Φ_1 changes sign at least once in $(0, -y_0]$. Letting $a \in (0, -y_0]$ be the smallest value such that $\Phi_1(0) = 0$ we get the contradiction

$$0 \leq \Lambda_1 \int_0^a w'(y)\Phi_1(y)dy = \Phi_1(a)w'(a) - \Phi_1(0)[-w''(0) + \kappa w'(0)] < 0, \tag{2.29}$$

and therefore $\Lambda_1 < 0$ for all $y_0 > y_{\min}(\kappa)$ which proves (v). □

Turning now to the NLEP (2.22) we first determine the critical value $\mu = \mu_c$ such that $\lambda = 0$. Assuming that $y_0 \neq y_c(\kappa)$ so that $-w''(0) + \kappa w'(0) \neq 0$ we note that the solution to

$$\mathscr{L}_{y_0}\phi = w^2, \quad y > 0; \quad \begin{cases} -\phi'(0) + \kappa\phi(0) = 0, \\ \phi(0) = 0, \end{cases} \text{ or } ; \quad \phi \to 0 \quad \text{as } y \to \infty,$$

is given by $\phi = w + \alpha w'$ where $\alpha = -\frac{-w'(0)+\kappa w(0)}{-w''(0)+\kappa w'(0)}$ (for the Dirichlet BC we take $\kappa \to +\infty$). Setting $\lambda = 0$ in the NLEP (2.22) we calculate that the critical $\mu = \mu_c$ is given by

$$\mu_c(y_0, \kappa) = \frac{\int_0^\infty w^2 dy}{\int_0^\infty w\mathscr{L}_{y_0}^{-1}w^2 dy} = \frac{\eta(y_0)}{\eta(y_0) - \frac{\alpha}{2}w(0)^2}, \tag{2.30}$$

where η is given in (2.6). An immediate consequence is the following lemma.

Lemma 2.2. *If $\mu \neq \mu_c$ then the NLEP (2.22) does not have a zero eigenvalue.*

Since $-w''(0) + \kappa w'(0) = 0$ at $y_0 = y_c$ we deduce that $y_0 = y_c$ is the only zero of μ_c in $y_0 > y_{\min}$ for all $\kappa \geq 0$ and furthermore it is easy to see that $\mu_c \gtrless 0$ for $y_0 \lessgtr y_c$. In Figure 1b we plot $\mu_c(y_0, \kappa)$ versus y_0 for different choices of $\kappa \geq 0$. In light of the preceding discussion we have the following conjectured stability result, the partial proof of which is provided in the remainder of this subsection.

Conjecture 2.1. *The NLEP (2.23) is stable if and only if $\mu > \mu_c(y_0, \kappa)$ for $y_0 < y_c$ and is stable for all $\mu \geq 0$ when $y_0 > y_c(\kappa)$.*

2.3.1. *Stability Results.* We determine sufficient conditions for the stability of (2.22) by using a continuation argument that starts with the known results in [7] for the case $\kappa = 0$ and $y_0 = 0$. Writing $\phi = \phi_R + i\phi_I$ and $\lambda = \lambda_R + i\lambda_I$ it can be shown that

$$\lambda_R = -\frac{L_1(\phi_R, \phi_R) + L_1(\phi_I, \phi_I)}{\int_0^\infty |\phi|^2 dy}, \tag{2.31a}$$

where

$$L_1(\phi, \phi) \equiv \int_0^\infty \left(|\phi'|^2 + \phi^2 - 2w\phi^2\right)dy + \mu\frac{\int_0^\infty w\phi dy \int_0^\infty w^2\phi dy}{\int_0^\infty w^2 dy}. \tag{2.31b}$$

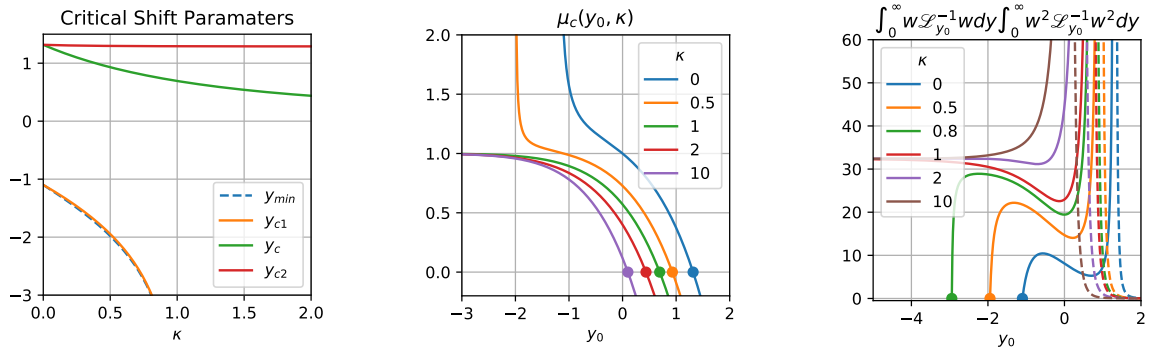

(A) (B) (C)

FIGURE 1. Plots of (A) important shift-parameter values, (B) the critical NLEP multiplier for which $\lambda = 0$ is an eigenvalue, and (C) plots of the integral $\int_0^\infty w\mathscr{L}_{y_0}^{-1}wdy \int_0^\infty w^2\mathscr{L}_{y_0}^{-1}w^2dy$ for $y_0 < y_c$ (solid) and $y_0 > y_c$ (dashed) while the solid dots indicate the values of $y_0 = y_{c1}$ at which these integrals vanish.

If $L_1(\phi, \phi) > 0$ for all $\phi \in H^1([0,\infty))$ then the NLEP (2.22) is clearly stable. In fact $L_1(\phi, \phi) > 0$ holds for all $\phi \in H^1([0,\infty))$ for $\mu = 2$ when $y_0 = 0$ and $\kappa = 0$. By perturbing y_0 and $\kappa \geq 0$ we can then determine a range of μ values for which the NLEP is linearly stable as described in the proceeding theorem. First however we note of the following useful identities

$$\mathscr{L}_{y_0}^{-1}w^2 = w + \alpha w', \mathscr{L}_{y_0}^{-1}w = w + \frac{1}{2}yw' + \beta w', \tag{2.32}$$

where

$$\alpha = \frac{w'(0) - \kappa w(0)}{-w''(0) + \kappa w'(0)}, \qquad \beta = \frac{\frac{3}{2}w'(0) - \kappa w(0)}{-w''(0) + \kappa w'(0)}, \tag{2.33}$$

with which we obtain

$$\int_0^\infty w\mathscr{L}_{y_0}^{-1}w^2\,dy = \int_0^\infty w^2\mathscr{L}_{y_0}^{-1}w\,dy = \int_0^\infty w^2\,dy - \frac{\alpha w(0)^2}{2}, \tag{2.34a}$$

$$\int_0^\infty w\mathscr{L}_{y_0}^{-1}w\,dy = \frac{3}{4}\int_0^\infty w^2\,dy - \frac{\beta w(0)^2}{2}, \tag{2.34b}$$

$$\int_0^\infty w^2\mathscr{L}_{y_0}^{-1}w^2\,dy = \int_0^\infty w^3\,dy - \frac{\alpha w(0)^3}{3}, \tag{2.34c}$$

where we have used

$$\int_0^\infty w^3\,dy = \frac{6}{5}\int_0^\infty w^2\,dy + \frac{3w(0)w'(0)}{5},$$

to simplify the last expression in (2.34). Numerically evaluating the above integrals we find that there exists a $y_{c1} \in (y_{\min}, y_c)$ such that $\int_0^\infty w\mathscr{L}_{y_{c1}}^{-1}wdy = 0$ for $0 \leq \kappa < 1$ and moreover

$$\int_0^\infty w\mathscr{L}_{y_0}^{-1}wdy \int_0^\infty w^2\mathscr{L}_{y_0}^{-1}w^2dy > 0,$$

only for $y_0 > y_{\min}$ (adopting the notation that $y_{\min} = -\infty$ for $\kappa \geq 1$) (see Figure 1c). We plot y_{c1} in Figure 1a and remark that it imposes a lower threshold on the shift parameter beyond which the continuation argument in the proof of the following theorem is no longer valid.

Theorem 2.1. *Let $\kappa \geq 0$ and $y_{c1}(\kappa) < y_0 < y_c(\kappa)$ where y_c is the critical shift parameter given by (2.18) and y_{c1} is the unique solution to $\int_0^\infty w\mathscr{L}_{y_0}^{-1}wdy = 0$ in $y_{min} < y < y_c$ for $0 \leq \kappa < 1$ and*

$y_{c1} = -\infty$ *for* $\kappa \geq 1$. *All eigenvalues of* (2.22) *are then stable if*

$$\mu_1(y_0, \kappa) < \mu < \mu_2(y_0, \kappa), \tag{2.35}$$

where

$$\mu_1(y_0, \kappa) \equiv \frac{2\int_0^\infty w^2 dy}{\int_0^\infty w\mathscr{L}_{y_0}^{-1}w^2 dy + \sqrt{\int_0^\infty w\mathscr{L}_{y_0}^{-1}w dy \int_0^\infty w^2\mathscr{L}_{y_0}^{-1}w^2 dy}}, \tag{2.36}$$

$$\mu_2(y_0, \kappa) \equiv \frac{2\int_0^\infty w^2 dy}{\int_0^\infty w\mathscr{L}_{y_0}^{-1}w^2 dy - \sqrt{\int_0^\infty w\mathscr{L}_{y_0}^{-1}w dy \int_0^\infty w^2\mathscr{L}_{y_0}^{-1}w^2 dy}}. \tag{2.37}$$

Proof. To prove the claim we follow the continuation argument of [31]. First, by the results in [17] we know that $L_1(\phi, \phi) > 0$ for all $\phi \in H^1([0, \infty))$ when $\mu = 2$, $\kappa = 0$, $y_0 = 0$ which by the above discussion implies that (2.22) is stable for $\mu = 2$. By the variational principle this also implies that the self-adjoint operator

$$L_1\phi = \mathscr{L}_{y_0}\phi - \frac{\mu}{2}\frac{\int_0^\infty w\phi dy}{\int_0^\infty w^2 dy}w^2 - \frac{\mu}{2}\frac{\int_0^\infty w^2\phi dy}{\int_0^\infty w^2 dy}w \tag{2.38}$$

is stable for $\mu = 2$. We then do continuation in $\kappa \geq 0$, $y_{\min}(\kappa) < y_0 < y_c(\kappa)$, and μ and assume that $L_1(\phi, \phi) > 0$ continues to hold for all $\phi \in H^1([0, \infty))$ until some point at which the principal eigenvalue of L_1 becomes zero and for which the corresponding eigenfunction is given by

$$\phi = \frac{\mu}{2}\frac{\int_0^\infty w\phi dy}{\int_0^\infty w^2 dy}\mathscr{L}_{y_0}^{-1}w^2 + \frac{\mu}{2}\frac{\int_0^\infty w^2\phi dy}{\int_0^\infty w^2 dy}\mathscr{L}_{y_0}^{-1}w. \tag{2.39}$$

Multiplying by w or w^2 and then integrating yields the system of equations

$$\begin{aligned}
\Big(\frac{\mu}{2}\frac{\int_0^\infty w\mathscr{L}_{y_0}^{-1}w^2 dy}{\int_0^\infty w^2 dy} - 1\Big)A + \frac{\mu}{2}\frac{\int_0^\infty w\mathscr{L}_{y_0}^{-1}w dy}{\int w^2 dy}B = 0,\\
\frac{\mu}{2}\frac{\int_0^\infty w^2\mathscr{L}_{y_0}^{-1}w^2 dy}{\int_0^\infty w^2 dy}A + \Big(\frac{\mu}{2}\frac{\int_0^\infty w^2\mathscr{L}_{y_0}^{-1}w dy}{\int_0^\infty w^2 dy} - 1\Big)B = 0,
\end{aligned} \tag{2.40}$$

for $A = \int_0^\infty w\phi dy$ and $B = \int_0^\infty w^2\phi dy$ and where we have used $\int_0^\infty w^2\mathscr{L}_{y_0}^{-1}w dy = \int_0^\infty w\mathscr{L}_{y_0}w^2 dy$. However this will have only a trivial solution if the determinant does not equal to zero and using using (2.34) we deduce that when $\mu = 2$, $\kappa = 0$, and $y_0 = 0$ the determinant equals $-9/10$. As a consequence the NLEP is stable provided the determinant is negative which is equivalent to (2.35). □

Due to the singularities of $\mathscr{L}_{y_0}^{-1}w$ and $\mathscr{L}_{y_0}^{-1}w^2$ when $y_0 = y_c(\kappa)$ the continuation starting from $\kappa = 0$, $y_0 = 0$, and $\mu = 2$ used in Theorem 2.1 cannot be extended to the region $y_0 > y_c(\kappa)$. However, by proving the stability of the NLEP (2.22) for all $\mu \geq 0$ sufficiently small when $y_0 > y_c(\kappa)$ we can proceed with a similar continuation argument. To proceed in this way we first need to establish the following lemmas.

Lemma 2.3. *Let* $r \geq 1$, $\kappa \geq 0$, $y_0 > y_c(\kappa)$, *and* $\lambda \geq 0$. *Then the solution to*

$$\mathscr{L}_{y_0}\phi - \lambda\phi = w^r, \qquad 0 < y < +\infty, \tag{2.41}$$

with $\phi \to 0$ *as* $y \to \infty$ *and either* $-\phi'(0) + \kappa\phi(0) = 0$ *or* $\phi(0) = 0$ *satisfies* $\phi < 0$.

Proof. Assume that $\phi > 0$ for $-\leq a < y < b \leq \infty$ with $\phi(b) = 0$, $\phi'(b) \leq 0$, and assume also for the moment that $a > 0$ so that $\phi(a) = 0$ and $\phi'(a) \geq 0$. Noting that $\mathscr{L}_{y_0}w' = 0$ we obtain the

contradiction.

$$0 > \int_a^b w^r w' dy + \lambda \int_a^b \phi w' dy = \int_a^b \big(w'(\mathscr{L}_{y_0} - \lambda)\phi - \phi(\mathscr{L}_{y_0} - \lambda)w'\big) dy$$
$$= w'(b)\phi'(b) - w'(a)\phi'(a) - w''(b)\phi(b) + w''(a)\phi(a) \geq 0,$$

where we have used that $w'(y) < 0$ for all $y \geq 0$. If instead $a = 0$ then if $\phi(a) = 0$ the same contradiction is achieved whereas if $\phi(0) > 0$ (only possible for mixed BCs) then we use the boundary condition $-\phi'(0) + \kappa\phi(0) = 0$ to get the contradiction

$$0 > -w'(a)\phi'(a) + w''(a)\phi(a) = -\phi(0)(-w''(a) + \kappa w'(a)) > 0.$$

□

A consequence of the above lemma is the following result.

Lemma 2.4. *If $y_0 > y_c(\kappa)$ and $\mu > 0$ then all real eigenvalues of (2.22) are stable.*

Proof. Letting λ be a real eigenvalue of (2.22) and ϕ the corresponding eigenfunction we write We have

$$\phi = \mu \frac{\int_0^\infty w\phi dy}{\int_0^\infty w^2 dy} (\mathscr{L}_{y_0} - \lambda)^{-1} w^2,$$

which upon multiplying by w and integrating gives the contradiction

$$1 = \mu \frac{\int_0^\infty w(\mathscr{L}_{y_0} - \lambda)^{-1} w^2 dy}{\int_0^\infty w^2 dy} < 0$$

by Lemma 2.3. □

From Lemma 2.3 and 2.4, we see that for $\mu > 0$ small sufficiently small the NLEP (2.22) is stable for all $y_0 > y_c(\kappa)$ and $\kappa \geq 0$. We vary μ until we reach some point where Hopf bifurcation (HB) occurs. By the same argument as in Theorem 2.1 we obtain the following result in the case of $y_0 > y_c(\kappa)$.

Theorem 2.2. *Let $\kappa \geq 0$ and $y_0 > y_c(\kappa)$ where y_c are given by (2.18). Then the eigenvalues of (2.22) are stable for all μ satisfying $0 \leq \mu \leq \mu_+(y_0, \kappa)$ where*

$$\mu_+(y_0, \kappa) \equiv \frac{2\int_0^\infty w^2 dy}{\left(\sqrt{\int_0^\infty w\mathscr{L}_{y_0}^{-1} w \int_0^\infty w^2 \mathscr{L}_{y_0}^{-1} w^2} - |\int_0^\infty w\mathscr{L}_{y_0}^{-1} w^2|\right)_+}, \tag{2.42}$$

and where $(z)_+ = z$ if $z > 0$ and 0 otherwise.

Proof. From (2.31) it suffices to determine the range of μ values such that $L_1(\phi, \phi) > 0$ for all $\phi \in H^1([0, \infty))$. By Lemma 2.4 this holds for sufficiently small values of $\mu \geq 0$. Proceeding as in the proof of Theorem 2.1 we recover the system (2.40) whose determinant is now *positive* when $\mu = 0$. Therefore the NLEP will remain stable as $\mu \geq 0$ is varied provided that the determinant remains positive and we write this condition explicitly as

$$\left(\frac{\mu}{2}\frac{\int_0^\infty w\mathscr{L}_{y_0}^{-1} w^2 dy}{\int_0^\infty w^2 dy} - 1\right)^2 - \left(\frac{\mu}{2}\right)^2 \frac{\int_0^\infty w\mathscr{L}_{y_0}^{-1} w dy}{\int_0^\infty w^2 dy} \frac{\int_0^\infty w^2\mathscr{L}_{y_0}^{-1} w^2 dy}{\int_0^\infty w^2 dy} > 0.$$

Using that $\int_0^\infty w\mathscr{L}_{y_0}^{-1} w^2 dy < 0$, $\int_0^\infty w\mathscr{L}_{y_0}^{-1} w dy < 0$, and $\int_0^\infty w^2\mathscr{L}_{y_0}^{-1} w^2 dy < 0$ by Lemma 2.3 we can rewrite this as

$$\mu\left(\sqrt{\int_0^\infty w\mathscr{L}_{y_0}^{-1} w dy \int_0^\infty w^2\mathscr{L}_{y_0}^{-1} w^2 dy} - \left|\int_0^\infty w\mathscr{L}_{y_0}^{-1} w^2 dy\right|\right) < 2\int_0^\infty w^2 dy.$$

If the term in the brackets on the left hand side is negative or zero then the NLEP is stable for all $\mu \geq 0$, and otherwise we obtain an upper bound for μ which proves the result. □

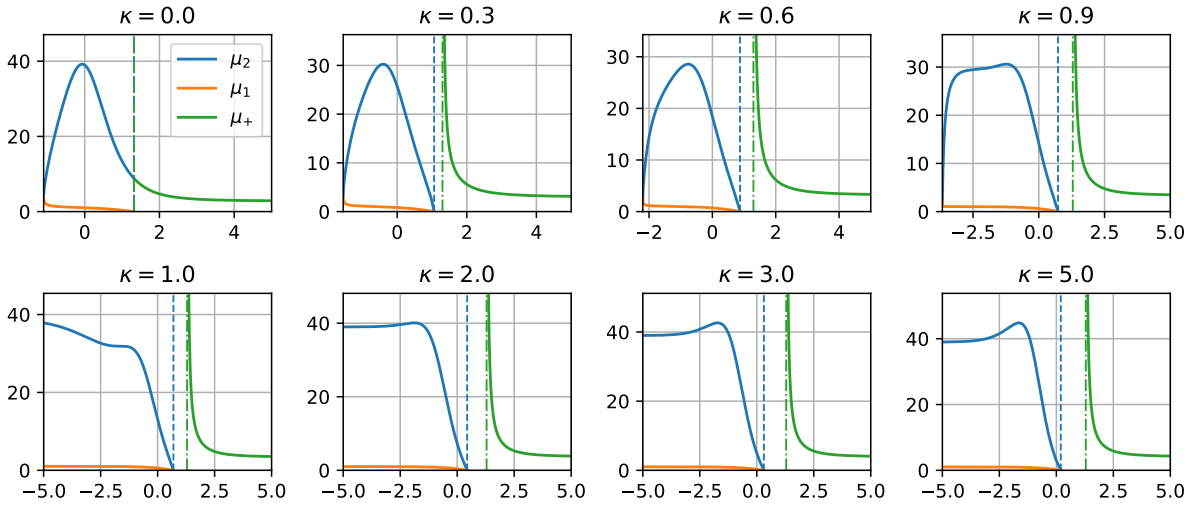

FIGURE 2. Plots of upper and lower stability bounds for μ. The legend in the top-left figure applies to all plots while the vertical dashed blue and dashed-dotted green line correspond to $y_0 = y_c$ and and $y_0 = y_{c2}$ respectively.

Using (2.34) we find that there exists a unique value $y_{c2} > y_c$ plotted in Figure 1a such that

$$\sqrt{\int_0^\infty w\mathscr{L}_{y_{c2}}^{-1}w \int_0^\infty w^2\mathscr{L}_{y_{c2}}^{-1}w^2} - \left|\int_0^\infty w\mathscr{L}_{y_{c2}}^{-1}w^2\right| = 0.$$

Moreover the quantity on the left-hand-side above is negative for $y_c < y_0 < y_{c2}$ and positive otherwise. Thus in the small interval $y_c < y_0 < y_{c2}$ the theorem states the problem is stable for all $\mu \geq 0$. We conjecture that this in fact holds for all $y_0 > y_c$, though the continuation used in the proof above establishes this only for $\mu < \mu_+(\kappa)$ for $y_0 > y_{c2}$.

2.3.2. *Instability Results.* Having established partial stability results we demonstrate next that the NLEP is unstable when $\mu < \mu_c$ for $y_{\min} < y_0 < y_c(\kappa)$. Note that when $y_0 > y_c(\kappa)$ then $\mu_c < 0$ and we conjecture that the NLEP is linearly stable for all $\mu \geq 0$ in this case.

Lemma 2.5. *If $y_{min}(\kappa) < y_0 < y_c(\kappa)$ and $\mu < \mu_c$ then the NLEP (2.22) has a positive real eigenvalue.*

Proof. By Lemma 2.1 the principle eigenvalue of the linearized operator $\mathscr{L}_{y_0}$ is positive $\Lambda_0 > 0$ and the corresponding eigenfunction Φ_0 is of one sign, while the second eigenvalue is strictly negative. If Λ_0 is an eigenvalue of the NLEP then we are done. Seeking instead a positive eigenvalue $\lambda \neq \Lambda_0$ we can rewrite (2.22) as

$$\phi = \mu\frac{\int_0^\infty w\phi dy}{\int_0^\infty w^2 dy}(\mathscr{L}_{y_0} - \lambda)^{-1}w^2.$$

Multiplying by w and integrating we obtain the equivalent expression $h(\lambda) = 0$ where

$$h(\lambda) \equiv \int_0^\infty w(\mathscr{L}_{y_0} - \lambda)^{-1}w^2 dy - \frac{\int_0^\infty w^2 dy}{\mu}. \tag{2.43}$$

Recalling the definition of μ_c in (2.30) we obtain $h(0) = \left(\mu_c^{-1} - \mu^{-1}\right)\int_0^\infty w^2 dy < 0$.

On the other hand we claim that $h(\lambda) \to +\infty$ as $\lambda \to \Lambda_0^-$. Indeed, letting ψ be the unique solution to

$$(\mathscr{L}_{y_0} - \lambda)\psi = w^2, \quad y > \infty,$$

with $\psi \to 0$ as $y \to \infty$ and either $-\psi'(0) + \kappa\psi(0) = 0$ or $\psi(0) = 0$. Writing $\psi = c_0\Phi_0 + \psi^\perp$ where $\int_0^\infty \Phi_0\psi^\perp dy = 0$ we obtain

$$(\mathscr{L}_{y_0} - \lambda)\psi^\perp = c_0(\lambda - \Lambda_0)\Phi_0 + w^2. \tag{2.44}$$

Multiplying by Φ_0 and integrating we calculate $c_0 = (\Lambda_0 - \lambda)^{-1}\int_0^\infty \Phi_0 w^2 dy$ and therefore

$$h(\lambda) = \frac{\int_0^\infty w^2\Phi_0 dy \int_0^\infty w\Phi_0 dy}{\Lambda_0 - \lambda} + \int_0^\infty w\psi^\perp dy - \mu^{-1}\int_0^\infty w^2 dy. \tag{2.45}$$

On the other hand, multiplying (2.44) by $\psi^\perp$ and integrating we can then use the variational characterization of the second eigenvalue of $\mathscr{L}_{y_0}$, which is negative by Lemma 2.1, to deduce that $\int_0^\infty w\psi^\perp dy$ is bounded as $\lambda \to \Lambda_0^-$ and therefore $h(\lambda) \to +\infty$ as $\lambda \to \Lambda_0^-$. By a continuity argument we then deduce the existence of an unstable eigenvalue of the NLEP (2.22) between 0 and Λ_0. □

In the remainder of this section we consider specific examples of one- and two-spike solutions for which we calculate their profiles and characterize their linear stability.

2.4. **Example: A One Boundary Spike Solution.** We consider an equilibrium solution in which a single spike concentrating at $x = -1$ is an equilibrium solution of (2.1a) with boundary conditions

$$-\varepsilon u_x + \kappa u = A, \quad x = -1, \qquad -\varepsilon u_x = 0, \quad x = 1. \tag{2.46}$$

Following §2.1 we find that

$$u \sim \xi_0 w_c\big(\tfrac{x+1}{\varepsilon} + y_0\big), \quad v \sim \xi_0 \operatorname{sech}\big(\tfrac{2}{\sqrt{D}}\big)\cosh\big(\tfrac{1-x}{\sqrt{D}}\big), \tag{2.47}$$

where ξ_0 and y_0 are given by (2.14b) with $l = 2$. The single spike solution is pinned to the left boundary and therefore does not undergo slow drift dynamics. Its linear stability is therefore governed solely by the $\mathcal{O}(1)$ eigenvalues of the NLEP (2.19) which is explicitly given by

$$\mathscr{L}_{y_0}\phi - \mu(\lambda)\frac{\int_0^\infty w_c(y+y_0)\phi(y)dy}{\int_0^\infty w_c(y+y_0)^2 dy} w_c(y+y_0)^2 = \lambda\phi, \tag{2.48}$$

where

$$\mu(\lambda) \equiv 2\frac{\tanh\frac{2}{\sqrt{D}}}{\sqrt{1+\tau\lambda}\tanh 2\sqrt{\frac{1+\tau\lambda}{D}}}. \tag{2.49}$$

We rewrite the NLEP as

$$\mathscr{A}(\lambda) = \frac{1}{\mu(\lambda)} - \mathscr{F}_{y_0}(\lambda) = 0, \quad \mathscr{F}_{y_0}(\lambda) \equiv \frac{\int_0^\infty w_c(y+y_0)(\mathscr{L}_{y_0} - \lambda)^{-1} w_c(y+y_0)^2 dy}{\int_0^\infty w_c(y+y_0)^2 dy}. \tag{2.50}$$

Using (2.34) we can calculate $\mathscr{F}_{y_0}(0)$ explicitly from which we find that $\mathscr{F}_{y_0}(0) > 1/2$ for all $y_{\min} < y_0 < y_c$ and $\mathscr{F}_{y_0}(0) < 0$ for all $y_0 > y_c$. In particular, we find that $\mathscr{A}(0) = 1/2 - \mathscr{F}_{y_0}(0)$ is strictly negative (resp. positive) for all $y_{\min} < y_0 < y_c$ (resp. $y_0 > y_c$). As a consequence, instabilities must arise through a HB. We seek conditions under which (2.50) admits unstable eigenvalues by using the argument principle. Specifically we let Γ_R be the counter-clockwise contour consisting of the semicircle $\{Re^{i\theta} | -\frac{\pi}{2} \le \theta \le \frac{\pi}{2}\}$ together with the segment $\{z = iy \,|\, -R \le y \le R\}$ of the imaginary axis. Then as $R \to \infty$ the change in the argument of $\mathscr{A}(\lambda)$ along Γ_R is determined by the number of zeros and poles of $\mathscr{A}(\lambda)$ having a positive real part. In view of Lemma 2.1 and noting that $\mu(\lambda) = \mathcal{O}(\lambda^{-1/2})$ and $\mathscr{F}_{y_0}(\lambda) = \mathcal{O}(\lambda^{-1})$ as $|\lambda| \to \infty$ with $\operatorname{Re}(\lambda) \ge 0$ we conclude that the number of unstable eigenvalues is given by

$$Z = \frac{1}{\pi}\Delta \arg \mathscr{A}(i\lambda_I)\Big|_{+\infty}^{0} + \begin{cases} 5/4, & y_0 < y_c(\kappa), \\ 1/4, & y_0 > y_c(\kappa) \end{cases}, \tag{2.51}$$

where $\Delta \arg \mathscr{A}(i\lambda_I)|_{+\infty}^0$ indicates the change in argument as λ_I varies from $+\infty$ to 0. The problem of finding the HB threshold is thus reduced to determining the behaviour of $\mathscr{A}(\lambda)$ on the imaginary

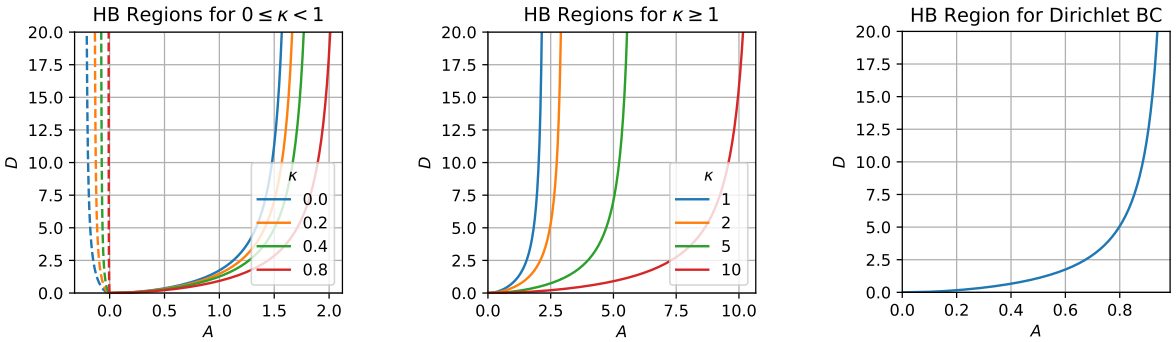

(A) (B) (C)

FIGURE 3. Boundaries for the existence of the Hopf bifurcation thresholds. Solid curves correspond to $A_c = q_c\sqrt{D}\tanh(2/\sqrt{D})$ for a single boundary spike solution for mixed BCs with (A) $0 \le \kappa < 1$ and (B) $\kappa \ge 1$, as well as for (C) Dirichlet BCs. In (A) the dashed curves indicate the existence threshold for a single spike solution $A > q_{\min}\sqrt{D}\tanh(2/\sqrt{D})$. In each of (A), (B), and (C) no Hopf bifurcation may occur if $A > A_c$, whereas a Hopf bifurcation threshold $\tau = \tau_h(D)$ may be computed for $A < A_c$.

axis. We have $\arg \mathscr{A}(i\lambda_I) = \pi/4$ as $\lambda_I \to \infty$ whereas $\mathscr{A}(0)$ is real valued. Furthermore, numerical calculations of $\mathrm{Re}\mathscr{A}(i\lambda_I)$ indicate that it is monotone decreasing in $\lambda_I > 0$ when it is positive. Since $\mathscr{A}(0) > 0$ when $y_0 > y_c$ this implies that $\Delta\mathscr{A}(i\lambda_I)\big|_{+\infty}^{0} = -\pi/4$ and therefore $Z = 0$. On the other hand since $\mathscr{A}(0) < 0$ when $y_0 < y_c$, from the monotonicity of $\mathrm{Re}\mathscr{A}(i\lambda_I)$ we deduce that there exists a unique value $\lambda_I^\star$ such that $\mathrm{Re}\mathscr{A}(i\lambda_I^*) = 0$. It follows that $\Delta\mathscr{A}(i\lambda_I)\big|_{+\infty}^{0} = 3\pi/4$ if $\mathrm{Im}\mathscr{A}(i\lambda_I^*) > 0$ or $\Delta\mathscr{A}(i\lambda_I)\big|_{+\infty}^{0} = -5\pi/4$ if $\mathrm{Im}\mathscr{A}(i\lambda_I^*) < 0$ in which case either $Z = 2$ or $Z = 0$ respectively. Therefore any instability arises from a HB and furthermore the HB threshold can be determined by calculating parameter values such that $\mathrm{Im}\mathscr{A}(i\lambda_I^*) = 0$.

The above discussion implies that a single spike solution is linearly stable if $y_0 > y_c$. In particular, using equation (2.14b) for the shift parameter in both the mixed and Dirichlet boundary condition cases it can be shown that $y_0 > y_c$ if and only if $A > A_c(D,\kappa)$ where

$$A_c(D,\kappa) = q_c\sqrt{D}\tanh(2/\sqrt{D}), \quad q_c(\kappa) = \begin{cases} \frac{2\kappa+\sqrt{\kappa^2+3}}{6-\kappa+\sqrt{\kappa^2+3}}\frac{3-\kappa+\sqrt{\kappa^2+3}}{3+\kappa-\sqrt{\kappa^2+3}}, & \text{(Mixed)}, \\ \frac{1}{2}, & \text{(Dirichlet)}. \end{cases} \tag{2.52}$$

Therefore $A \le q_c\sqrt{D}\tanh(2/\sqrt{D})$ is a necessary condition for the single spike solution to undergo a HB and in Figure 3 we plot the boundaries of this region for select values of $0 \le \kappa < 1$, $\kappa \ge 1$, as well as for Dirichlet BCs.

Before calculating the HB threshold for general parameter values it is instructive to first consider the shadow limit obtained by letting $D \to \infty$. The region for which HB thresholds may be calculated then becomes $A < 2q_c$ (in addition to $A > 2q_{\min}$ when $0 \le \kappa < 1$). Furthermore, since $\mu(i\lambda_I) \sim 2(1+i\tau\lambda_I)^{-1}$ we obtain the simplified equations for the HB threshold

$$1 - 2\mathrm{Re}\mathscr{F}_{y_0}(i\lambda_I) = 0, \qquad \tau\lambda_I - 2\mathrm{Im}\mathscr{F}_{y_0}(i\lambda_I) = 0,$$

to be solved for $\lambda_I = \lambda_h^\infty(A)$ and $\tau = \tau_h^\infty(A)$. In fact it suffices to numerically solve the first equation for $\lambda_h^\infty(A)$, with the second equation immediately giving us $\tau_h^\infty(A)$. By the preceding discussion we also determine that the single-spike pattern is unstable with respect to a HB when $\tau > \tau_h^\infty(A)$ (since $\mathrm{Im}\mathscr{A}(i\lambda_h^\infty) > 0$ in this case) and is linearly stable otherwise. Using the shadow

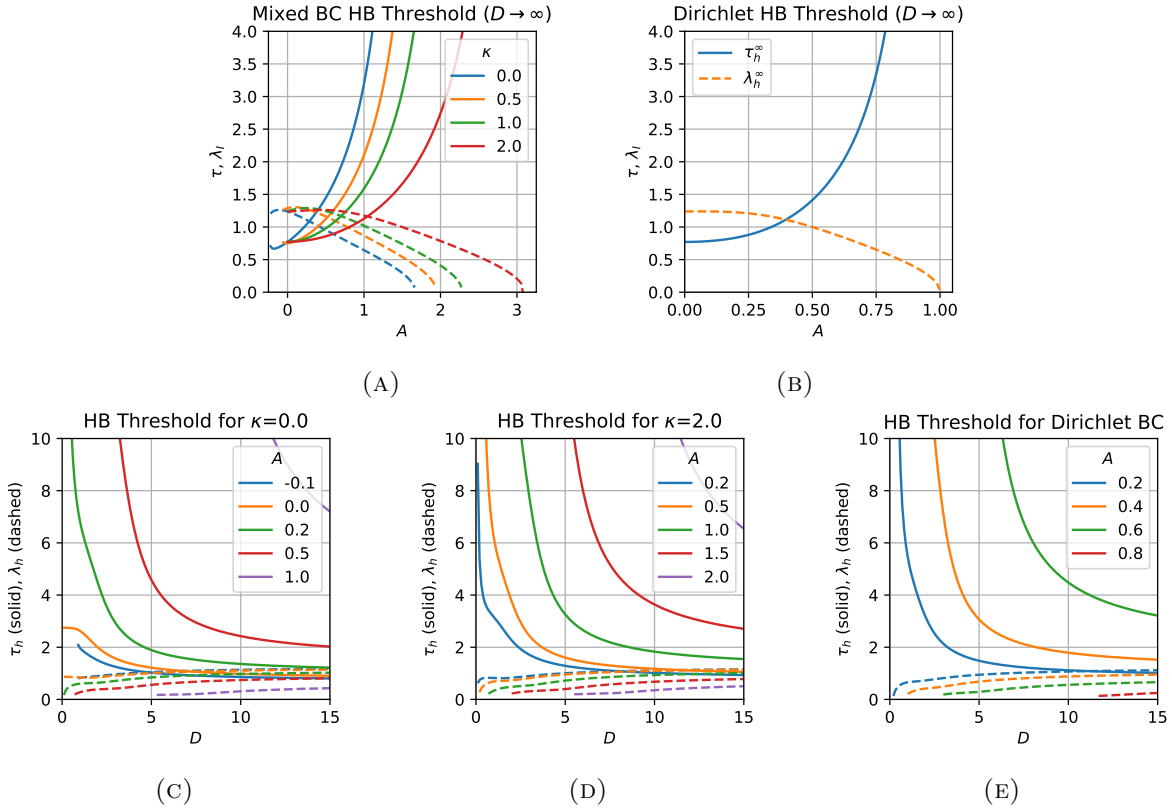

FIGURE 4. Plots of the Hopf bifurcation threshold (solid) and corresponding eigenvalue (dashed) as functions of A in the shadow limit for (A) mixed and (B) Dirichlet BCs. Similar plots of the HB and eigenvalue as a function of D for mixed BCs with (C) $\kappa = 0$, (D) $\kappa = 2$, and for (E) Dirichlet BCs. In all plots the single spike solution undergoes a Hopf bifurcation as τ exceeds τ_h.

limit threshold as an initial guess, we can then numerically continue the HB threshold $\tau_h(D, A)$ by decreasing D from a large value for which the shadow limit provides a suitable approximation. In Figures 4a and 4b we plot the HB threshold and corresponding eigenvalue in the shadow limit for both mixed and Dirichlet BCs respectively. Similarly in Figures 4c, 4d, and 4e we plot $\tau_h(D, A)$ and $\lambda_h(D, A)$ for $\kappa = 0$, $\kappa = 2$, and for Dirichlet BCs respectively. Finally in Figure 5 we plot $v(-1, t)$ obtained by numerically solving (2.1) using FlexPDE 6 [20] for different values of $\tau > 0$ and using the single spike solution at the given parameter values of $D = 4$, $A = 0.2$, $\varepsilon = 0.005$, and κ as the initial condition. These plots, together with more numerical simulations (not shown) support our calculated stability thresholds.

2.5. **Example: Two Boundary Spikes.** Suppose that $A_- = A_+ = A$ and consider an equilibrium solution in which two-spikes concentrate at the endpoints $x = -1$ and $x = +1$. Following (2.1.1) such a two-spike equilibrium solution is given by (2.13) with $l_- = l$ and $l_+ = 2 - l$ where $0 < l < 2$ satisfies the algebraic equation (2.15b) which we write explicitly as

$$\eta(y_+) \tanh \tfrac{l}{\sqrt{D}} \cosh \tfrac{2-l}{\sqrt{D}} - \eta(y_-) \tanh \tfrac{2-l}{\sqrt{D}} \cosh \tfrac{l}{\sqrt{D}} = 0 \tag{2.53}$$

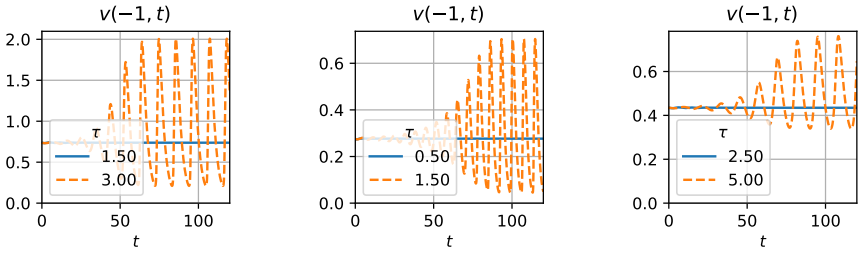

(A) Neumann BCs, $D = 5.0$, $A = 0.20$

(B) $\kappa = 2.0$, $D = 5.0$, $A = 0.20$

(C) Dirichlet BCs, $D = 5.0$, $A = 0.20$

FIGURE 5. Inhibitor values at $x = -1$ obtained by numerically simulating (2.1a) with boundary conditions (2.46) using FlexPDE 6 [20] where $\varepsilon = 0.005$ and the remaining values of A, D, τ, and κ are indicated in the figure and their individual captions.

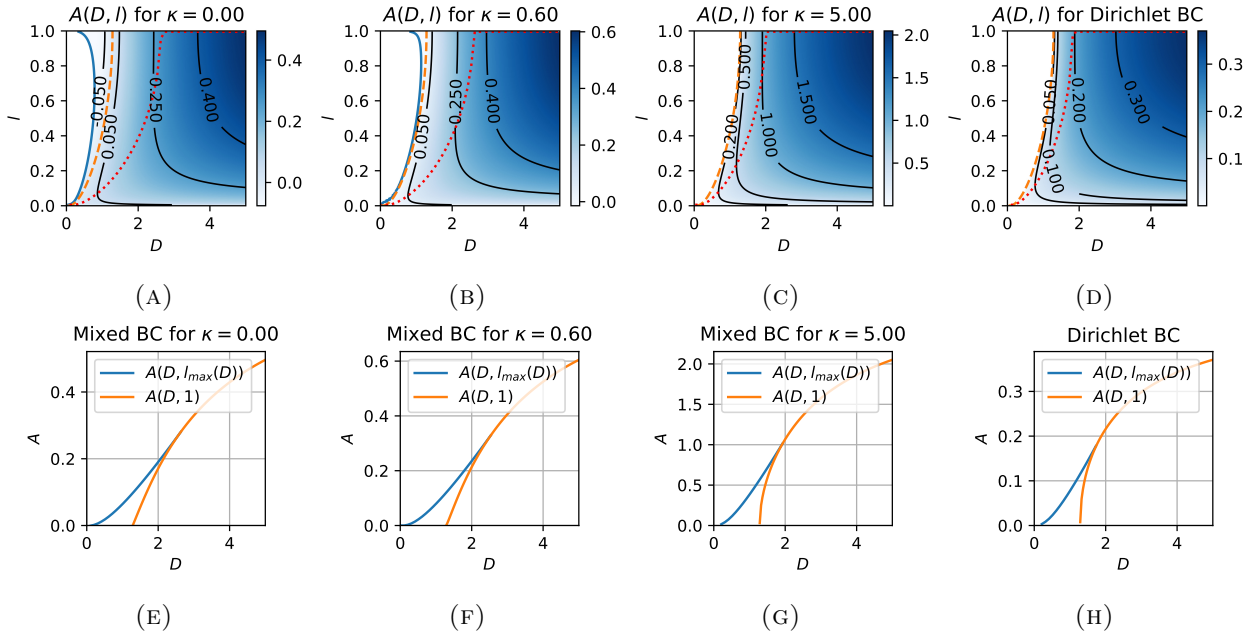

(A) (B) (C) (D)

(E) (F) (G) (H)

FIGURE 6. (A)-(D) Plots of $A = A(D, l)$ obtained by solving (2.53) for A as a function of $D > 0$ and $0 < l < 1$. The dashed orange curves correspond to values where $A = 0$ in (A) and (B) and where $A \to 0^+$ in (C) and (D). The dotted red curve indicates the values where of $l = l_{\max}$ where A is maximized for a given value of D. Note that there is a threshold value of D beyond which $l_{\max} = 1$. In (E)-(H) we plot the values of A obtained along the curves $l = 1$ (for D beyond some threshold) and along $l = l_{\max}$ as a function of D.

where

$$y_{\pm} = \begin{cases} \log\left(\frac{1-\kappa+3q_{\pm}+\sqrt{(1-\kappa+3q_{\pm})^2+4(1+\kappa)q_{\pm}}}{2(1+\kappa)}\right), & 0 \le \kappa < \infty \\ \log\left(\frac{3q_{\pm}-1+\sqrt{(3q_{\pm}-1)^2+4q_{\pm}}}{2}\right), & \text{Dirichlet BCs.} \end{cases} \tag{2.54a}$$

and

$$q_- = \frac{A}{\sqrt{D}}\coth\frac{l}{\sqrt{D}}, \quad q_+ = \frac{A}{\sqrt{D}}\coth\frac{2-l}{\sqrt{D}}. \tag{2.54b}$$

Note that $l = 1$ is always a solution to (2.53) and this yields a a symmetric two-spike solution in which both boundary spikes are identical for all $A > \sqrt{D}q_{\min}(\kappa)\tanh(1/\sqrt{D})$ and $D > 0$. The remaining asymmetric solutions correspond to solutions of (2.53) with $0 < l < 1$ (or equivalently $1 < l < 2$). Note that from (2.15b) we calculate $\xi_-/\xi_+ = \mathrm{sech}((2-l)/\sqrt{D})/\mathrm{sech}(l/\sqrt{D})$ so that $\xi_- < \xi_+$ when $0 < l < 1$. To find such asymmetric solutions we need to numerically solve (2.53) for $l = l(A, D)$. However, as previously observed in [7] for specific values of D and A this possesses two distinct solution. It is therefore more convenient to numerically solve for $A = A(D, l)$ for fixed values of $D > 0$ and $0 < l < 1$ as outlined below.

Our method for numerically calculating $A(D, l)$ differs in the cases $0 \le \kappa < 1$ and $\kappa > 1$ (the latter including the formal limit $\kappa \to \infty$ corresponding to Dirichlet BCs). In the former we may substitute $A = 0$ into (2.53) to obtain a κ-independent equation which we can solve for $D = D_0(l)$. It is then straightforward to calculate $A = A(D, l)$ for fixed values of l using numerical continuation in D starting from $D = D_0(l)$ for which $A = 0$. Note than when decreasing A the existence constraint $A > \sqrt{D}q_{\min}(\kappa)\tanh((2-l)/\sqrt{D})$ must be satisfied where $q_{\min}$ is given by (2.16). On the other hand, since A must be strictly positive when $\kappa \ge 1$ we instead first consider the shadow limit $D \to \infty$ for which $q_- \to A/l$ and $q_+ \to A/(2-l)$ and with which we numerically solve (2.53) for $A = A(\infty, l)$. For finite values of $D > 0$ we can solve (2.53) for $A = A(D, l)$ by again using numerical continuation in D but this time starting from a large value for which $A(\infty, l)$ is a good approximation.

In Figures 6a-6d we plot $A = A(D, l)$ for mixed BCs at select values of $0 \le \kappa < \infty$ as well as for Dirichlet BCs. In each plot the dashed orange curves correspond to $D = D_0(l)$ while the dotted red curves correspond to the values of $l = l_{\max}(D)$ along which $A(D, l)$ is maximized at each $D > 0$. Note that $l_{\max}(D) = 1$ beyond some value of $D > 0$. Moreover the solid blue curves in Figures 6a and 6b indicate the existence threshold given by the intersection of $A = A(D, l)$ and $A = \sqrt{D}q_{\min}(\kappa)\tanh((2-l)/\sqrt{D})$. Interestingly, as can be seen in Figures 6a-6d, and as previously highlighted in [7], there is a finite range of D values for which two distinct asymmetric solutions can be constructed for a fixed value of $A > 0$: one with $l < l_{\max}(D)$ and the other with $l > l_{\max}(D)$. Values of $A > 0$ and $D > 0$ for which two such asymmetric solutions can be constructed lie in the region between the curves $A(D, l_{\max}(D))$ and $A(D, 1)$ as indicated in Figures 6e - 6h. If $A > A(D, l_{\max}(D))$ then there are no asymmetric two-spike solutions and only a symmetric solution can be constructed, whereas if $A < A(D, 1)$ then there is exactly one asymmetric solution. Note that $A(D, 1)$ is bounded and approaches a horizontal asymptote as $D \to \infty$ which can be numerically calculated. Finally we neglect asymmetric solutions with $A < 0$ since, as seen below, they are always linearly unstable.

By assuming that τ is sufficiently small we can assume that there are no HBs and therefore focus solely on instabilities that arise from an eigenvalue of the NLEP (2.19) crossing the origin into the right half-plane where the real-part is positive, i.e. the so-called competition instabilities. As described in [29] and [7] the NLEP (2.19) admits a zero eigenvalue only when the Jacobian of $\boldsymbol{B}$ in (2.8) is singular. In particular, differentiating (2.8) with respect to l it can be shown (see [7]) that for $0 < l < 1$ the NLEP (2.19) admits a zero eigenvalue along the curves where $\partial_l A(D, l) = 0$, that is when $l = l_{\max}(D)$ and $l = 1$. Moreover, since asymmetric two spike solutions are unstable along $A = 0$ and $D = D_0(l)$ (see Appendix C of [7]) we can deduce that only those asymmetric solutions with $0 < l < l_{\max}(D)$ are linearly stable. Similarly, we can deduce that the symmetric two-spike solutions are stable for $A > A(D, 1)$ and unstable otherwise. In light of this the curves $A = A(D, 1)$ and $A = A(D, l_{\max}(D))$ in Figures 6e-6h separate the $A > 0$ and $D > 0$ values into three distinct regions. Fist, in the region $A > A(D, l_{\max}(D))$ the symmetric two-spike solution is stable and there are no asymmetric solutions. Second in the region bounded by $A = A(D, l_{\max}(D))$

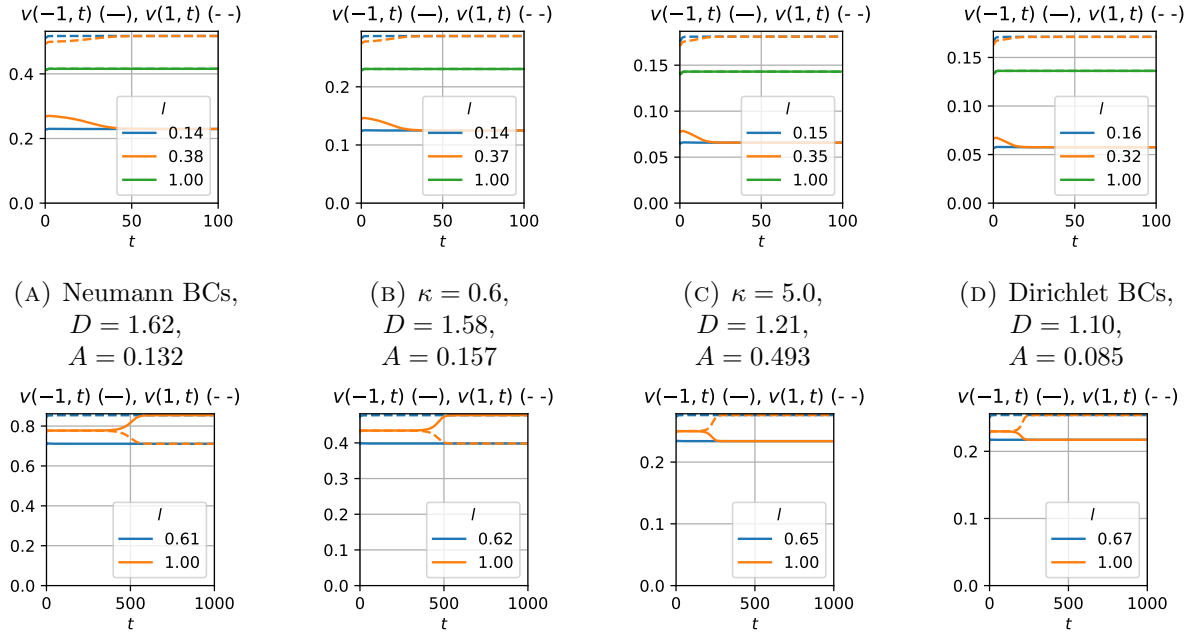

(A) Neumann BCs, $D = 1.62$, $A = 0.132$

(B) $\kappa = 0.6$, $D = 1.58$, $A = 0.157$

(C) $\kappa = 5.0$, $D = 1.21$, $A = 0.493$

(D) Dirichlet BCs, $D = 1.10$, $A = 0.085$

(E) Neumann BCs, $D = 4$, $A = 0.408$

(F) $\kappa = 0.6$, $D = 4$, $A = 0.499$

(G) $\kappa = 5$, $D = 4$, $A = 1.770$

(H) Dirichlet BCs, $D = 4$, $A = 0.326$

FIGURE 7. Values of $v(-1,t)$ (solid) and $v(+1,t)$ (dashed) obtained by numerically solving (2.1) using FlexPDE 6 [20] and using the two boundary spike solutions obtained using the gluing with the indicated values of values of l, $A > 0$, $D > 0$, and κ as an initial condition. The remaining problem parameters used are $\varepsilon = 0.005$ and $\tau = 0.2$.

and $A = A(D,1)$ both the symmetric two-spike solution and a unique asymmetric solutions are linearly stable. Finally in the region $A < A(D,1)$ the symmetric two-spike solution is linearly unstable and there is a unique stable asymmetric two solution.

In Figures 7 we plot the values of $v(\pm,t)$ obtained by numerically solving (2.1) using FlexPDE 6 [20] for several values of $A > 0$ and $D > 0$. The initial condition used in each simulation is obtained by using the value of $l > 0$ obtained by solving (2.53) and indicated in the legend. In particular, in the top row of Figure 7 the values of $A > 0$ and $D > 0$ are chosen in the region where the system possesses one stable symmetric solution and two asymmetric solutions: one stable solution with $l < l_{\max}$ and the other an unstable solution with $l_{\max} < l < 1$. The plots illustrate how the solution with $l_{\max} < l < 1$ is destabilized in finite time, and furthermore appears to settle to the stable asymmetric solution with $l < l_{\max}$. On the other hand, in the bottom row of Figure 7 we choose values of $A > 0$ and $D > 0$ for which the symmetric solution is linearly unstable and for which a unique stable asymmetric solution can be constructed. The resulting numerical solutions illustrate that the symmetric solution is unstable and furthermore collapses to the stable asymmetric solution in finite time. As highlighted in [7] this behaviour suggests the association of the boundary spike with the smaller value of l with a boundary layer. Indeed, in the absence of inhomogeneous boundary conditions a two-spike solution undergoing a competition instability becomes a one-spike solution. However since a one-spike solution cannot simultaneously satisfy both inhomogeneous boundary conditions a second boundary-bound spike must persist. The association of this boundary layer with the spike corresponding to the smaller value of l is supported by the

plots of $A(D,l)$ in Figures 6a-6d which show that the stable asymmetric solution emerges from $l=0$ as A is increased from zero.

Interestingly, the symmetric two-spike solution constructed above has an analogous symmetric solution in higher-dimensional bounded domains consisting of a one-dimensional boundary-bound spike extended along the domain's boundary. As discussed in more detail in the next section these boundary-layer solutions have qualitatively similar stability properties to their one-dimensional counterparts. In particular these solutions become unstable as the inhomogeneous term A is decreased below some critical threshold (c.f. Figures 6e-6h). However, rather than leading to the collapse of one of the spikes as in a one-dimensional domain, a behaviour that is made impossible by the connectivity of the domain's boundary in dimensions greater than two, the instability of the boundary layer solution instead leads to a composite solution consisting of both a boundary layer and a near-boundary spike (see Figure 9).

3. Boundary Layer Solutions in the Shadow Limit in $\Omega \subset \mathbb{R}^N$ $(N \geq 2)$

We now consider the existence and linear stability of boundary layer solutions to (1.1) in the so-called shadow limit obtained by taking the limit $D \to \infty$. Assuming that Ω is connected then in such a limit V formally approaches a constant value $V \sim \xi$ so that by integrating the second equation in (1.1a) and using the divergence theorem we obtain the shadow system

$$U_t = \varepsilon^2 \Delta U - U + \frac{U^2}{\xi}, \quad \tau \xi_t = -\xi + \frac{1}{\varepsilon|\Omega|}\int_\Omega U^2 dx, \qquad x \in \Omega,\ t>0 \tag{3.1a}$$

with either mixed or Dirichlet boundary condition

$$\begin{cases} \varepsilon \partial_\nu U + \kappa U = A, & \text{for } x \in \partial\Omega,\ t>0, \text{ or} \\ U = A & \text{for } x \in \partial\Omega,\ t>0. \end{cases} \tag{3.1b}$$

Steady state solutions of (3.1) satisfy the system

$$\begin{aligned} &\varepsilon^2 \Delta U - U + \frac{U^2}{\xi} = 0, \qquad \xi = \frac{1}{\varepsilon|\Omega|}\int_\Omega U^2 dx, && x \in \Omega \\ &\varepsilon \partial_\nu U + \kappa U = A, && x \in \partial\Omega. \end{aligned} \tag{3.2}$$

for which we seek to construct positive boundary layer solutions $(U_\varepsilon, \xi_\varepsilon)$ for small $\varepsilon > 0$.

3.1. The existence of boundary layer solutions.

Using the change of variables $x = \varepsilon y$ and letting $U = \xi u$ and $a = A/\xi$, problem (3.2) reduces to the following scalar problem

$$\begin{aligned} &\Delta_y u - u + u^2 = 0, && x \in \Omega_\varepsilon, \\ &\partial_{\nu_y} u + \kappa u = a, && x \in \partial\Omega_\varepsilon. \end{aligned} \tag{3.3}$$

where $\Omega_\varepsilon \equiv \{y \in \mathbb{R}^N \,|\, \varepsilon y \in \Omega\}$ and ν_y is the outward unit normal to $\partial\Omega_\varepsilon$ at $y = \varepsilon^{-1}x \in \partial\Omega_\varepsilon$.

Recall from our analysis of the one-dimensional problem above that $y_c(\kappa)$ given by (2.18) is the unique (positive) value of y at which $-w_c'(y) + \kappa w_c(y)$ is maximized. Denote this maximum value by $a_{\max}(\kappa) \equiv -w_c'(y_c(\kappa)) + \kappa w_c(y_c(\kappa))$. Then for any $0 \leq a < a_{\max}(\kappa)$ we can define

$$w_a(s) \equiv w_c(s + y_a), \tag{3.4}$$

where w_c is given by (2.4) and y_a is the unique solution to

$$-w_c'(y_a) + \kappa w_c(y_a) = a, \qquad y_0 > y_c(\kappa).$$

In the remainder of this section we will use the method of sub- and super-solutions to prove the following existence existence result.

Theorem 3.1. *Let $\kappa \geq 0$ be arbitrary and assume that $A > 0$ satisfies*

$$A > A_{min}(\kappa) \equiv \frac{|\Omega|}{|\partial\Omega|} \frac{-w_c'(y_c(\kappa)) + \kappa w_c(y_c(\kappa))}{\int_{y_c(\kappa)}^{\infty} w_c^2(s)ds}, \tag{3.5}$$

where w_c is given by (2.4) and y_c is the critical shift parameter given by (2.18). Then there exists an $\varepsilon_0 > 0$ such that for all $0 < \varepsilon < \varepsilon_0$ problem (3.1) has a positive steady state solution $(U_\varepsilon, \xi_\varepsilon)$ satisfying

$$U_\varepsilon(x) = \xi_\varepsilon(w_a(h/\varepsilon) + \mathcal{O}(\varepsilon)), \tag{3.6}$$

$$\xi_\varepsilon \sim \frac{|\Omega|}{|\partial\Omega|} \left[\int_0^\infty w_a^2(s)ds\right]^{-1}, \tag{3.7}$$

where $h = \text{dist}(x, \partial\Omega)$, $w_a = w_c(y + y_a)$, and y_a is the unique solution to the nonlinear equation

$$\frac{-w_c'(y_a) + \kappa w_c(y_a)}{\int_{y_a}^{\infty} w_c^2(s)ds} = \frac{|\partial\Omega|}{|\Omega|} A, \qquad on \quad y_c(\kappa) < y_a < \infty. \tag{3.8}$$

We make the following remarks.

Remark 3.1. *The proof of Theorem 3.1 given below utilized the method of sub- and super-solutions and relies on the stability of a certain linearized operator which holds only when $y_a > y_c$. For this reason we assume in the theorem that $y_a > y_c$ and since the left-hand-side of (3.8) is monotone increasing in y_a for $y_a > y_c$ this imposes the lower bound (3.5). We note that (3.6) and (3.7) can be formally shown to hold for values of $A < A_{min}$ by using the method of matched asymptotic expansions. However these solutions are expected to be linearly unstable since the local linearized operator contains a unstable eigenvalue which produces resonance when embedded in higher dimensions (see [18]). This is supported by our numerical calculations in Section 3.3.*

Remark 3.2. *When the boundary condition (3.1b) are replaced with the Dirichlet boundary condition $U = A$ on $\partial\Omega$ the above theorem continues to hold with the following modifications obtained by replacing A with κA and formally taking the limit $\kappa \to \infty$. Since the critical shift parameter $y_c = 0$ for Dirichlet BCs the constraint for A and nonlinear equation for y_a are respectively replaced with*

$$A > A_{min} \equiv \frac{1}{2}\frac{|\Omega|}{|\partial\Omega|}, \qquad \frac{w_c(y_a)}{\int_{y_a}^{\infty} w_c^2(s)ds} = \frac{|\partial\Omega|}{|\Omega|} A, \qquad on \quad y_c(\kappa) < y_a < \infty. \tag{3.9}$$

Before proving Theorem 3.1 we first establish the following geometric results.

3.1.1. *Geometric Preliminaries: Fermi Coordinates and the Laplace-Beltrami Operator.* To present and prove our results we first collect the following notation and results from Riemannian geometry similar to that of Section 3 of [19]. For a fixed $\gamma \in (0, 1)$ let

$$J_\varepsilon = \{x \in \bar{\Omega} : \text{dist}(x, \Gamma) < \varepsilon^\gamma\},$$

where $\text{dist}(x, \Gamma)$ denotes the Euclidean distance of a point $x \in \mathbb{R}^N$ to the manifold Γ. Note that for small $\varepsilon > 0$ the region J_ε is part of the normal bundle of Γ which we denote by $\mathbf{N}\Gamma$. The normal bundle $\mathbf{N}\Gamma$ is endowed with the metric $\bar{g}$ induced from its embedding into $\mathbb{R}^N$. Specifically

$$\bar{g} = g^T + g^h,$$

where g^T is the metric of Γ induced from its embedding into $\mathbb{R}^N$ and $g^h \equiv dh^2$ is the Euclidean metric on the normal fibres

In a neighbourhood of a given point $P \in \Gamma$, the inward unit normal $\nu(P)$ together with an orthonormal frame in the tangent bundle $T\Gamma$ can be viewed as a moving orthonormal frame in a neighbourhood of $(P, 0) \in \Gamma \times \mathbb{R}$. We can then define a local parametrization from a neighbourhood of $(P, 0) \in \Gamma \times \mathbb{R}$ into a neighbourhood of $y \in \mathbb{R}^N$ by

$$\Phi(P, h) \equiv P + h\nu(P).$$

Let $(t_1,\dots,t_{N-1}) \longmapsto P(t_1,\dots,t_{N-1})$ be a parametrization of Γ close to a given point $P_\bullet$ for which we assume, without loss of generality, that $P(0)=P_\bullet$. To keep the notation short we suppress the explicit dependence of $\nu(P)$ on P and denote it simply by ν. Hence

$$X(t_1,\dots,t_{N-1},h) \equiv Y(t_1,\dots,t_{N-1}) + h\nu(t_1,\dots,t_{N-1}) \tag{3.10}$$

where $Y(t_1,...,t_{N-1}) = (Y_1,Y_2,...,Y_N) \in \mathbb{R}^N$ with $Y(0)=P_\bullet$ is a parametrization of $\mathbb{R}^N$ close to $P_\bullet$. For the remainder of the paper we will refer to $(t_1,\dots,t_{N-1},h)$ as the *Fermi coordinates* in the neighbourhood of $P_\bullet$. Using the Fermi coordinates any point $X \in J_\varepsilon$ can be represented as

$$X = Y + h\nu(Y), \quad Y \in \Gamma, \quad 0 \le h < \varepsilon^\gamma,$$

and in this parametrization the Euclidean metric, or more precisely the pull-back of g by Φ, is close to the induced metric on $N\Gamma$ by the following lemma.

Lemma 3.1. *In the above-defined coordinates,*

$$\Phi^* g = \bar{g} + h(\Theta + 2\hat{\Theta}) + h^2\tilde{\Theta},$$

where Θ and $\tilde{\Theta}$ are tensors acting on $T\Lambda$ and have coefficients which are smooth functions on Λ.

Proof. Recall that (3.10) is a parametrization of $\mathbb{R}^N$ close to $P_\bullet$. To compute the coefficients of the Euclidean metric in these coordinates it is enough to compute $\partial_{t_i}X\cdot\partial_{t_j}X$, $\partial_{t_i}X\cdot\partial_h X$, and $\partial_h X\cdot\partial_h X$. Observe that $\partial_{t_i}Y$ is a tangent vector to Γ while ∂_h is a normal vector to Γ and hence $\partial_{t_i}Y\cdot\nu\equiv 0$. Using this it is easy to check that

$$\partial_{t_i}X\cdot\partial_{t_j}X = \partial_{t_i}Y\cdot\partial_{t_j}Y + h\left(\partial_{t_i}Y\cdot\partial_{t_j}\nu + \partial_{t_j}Y\cdot\partial_{t_i}\nu\right) + h^2\partial_{t_i}\nu\cdot\partial_{t_j}\nu$$
$$\partial_{t_i}X\cdot\partial_h X = h\partial_{t_i}Y\cdot\nu, \qquad \partial_h X\cdot\partial_h X = \nu\cdot\nu.$$

We then set

$$\Theta \equiv \sum_{i,j=1}^{N-1}\left(\partial_{t_i}Y\cdot\partial_{t_j}\nu + \partial_{t_j}Y\cdot\partial_{t_i}\nu\right)dt_i dt_j,$$
$$\hat{\Theta} \equiv \sum_{i=1}^{N-1}\partial_{t_i}Y\cdot\nu dt_i dh, \qquad \tilde{\Theta} \equiv \sum_{i,j=1}^{k}\partial_{t_i}\nu\cdot\partial_{t_j}\nu dt_i dt_j,$$

and observe that the coefficients of Θ, $\hat{\Theta}$, and $\tilde{\Theta}$ are smooth functions on Γ. With this notation, we can then write

$$g = \sum_{i,j=1}^{N-1}\left((g^T)_{ij} + h\Theta_{ij} + h^2(\tilde{\Theta})_{ij}\right)dt_i dt_j + 2\sum_{i=1}^{N-1}h(\hat{\Theta})_{iN}dt_i dh + dh^2, \tag{3.11}$$

which completes the proof of the lemma. □

Recall that if the metric tensor on a manifold M is given in local coordinates by $g=\sum_{i,j=1}^m g_{ij}dx_i dx_j$ and f is a (smooth) function defined on M then the gradient and the Laplace-Beltrami operator acting on f are respectively given by

$$\nabla_g f = \sum_{i,j=1}^{N}\left(g^{ij}\partial_{x_i}f\right)\partial_{x_j}, \quad \Delta_g f \equiv \frac{1}{\sqrt{\det g}}\sum_{i,j=1}^{N}\partial_{x_i}\left(\sqrt{\det g}\,g^{ij}\partial_{x_j}f\right)$$

where $\left(g^{ij}\right)$ is the inverse matrix of the matrix (g_{ij}). When $\varepsilon>0$ is sufficiently small we can use the expansion of g in Lemma 3.1, especially formula (3.11), to obtain the following decomposition of the Euclidean Laplacian in J_ε.

Lemma 3.2. *The Euclidean Laplacian Δ in J_ε can be decomposed as*

$$\Delta \equiv \sum_{i=1}^{N} \partial_{x_i}^2 = \Delta_{\bar g} + D,$$

where $\Delta_{\bar g} = \Delta_{g^T} + \partial_{hh}^2$ denotes the Laplace-Beltrami operator on J_ε (seen as part of the normal bundle of Γ) for the metric $\bar g = g^T + g^h$, and D is a second-order differential operator which, in Fermi coordinates, can be expanded as

$$D = hD^{(2)} + D^{(1)}$$

where $D^{(2)}$ (respectively $D^{(1)}$) are second-order (respectively first-order) partial differential operators whose coefficients are smooth and bounded in J_ε.

The Euclidean gradient ∇ in J_ε can be decomposed as

$$\nabla \equiv \sum_{i=1}^{N} \partial_{x_i}(\cdot)\partial_{x_i} = \nabla_{\bar g} + h\tilde D$$

where $\nabla_{\bar g} = \nabla_{g^T} + \partial_h(\cdot)\partial_h$ denotes the gradient operator on J_ε for the metric $\bar g = g^T + g^h$, and $\tilde D$ is a first-order partial differential operators, whose coefficients are smooth and bounded in J_ε.

Finally, we can define in a fixed tubular neighbourhood of Γ the function χ by

$$\mathrm{dvol}_g = \chi \mathrm{dvol}_{\bar g} = \chi \mathrm{d}\sigma \mathrm{d}h, \tag{3.12}$$

where σ is the volume element of Γ. Such a χ is smooth and $\chi \equiv 1$ along Γ. Moreover, it follows from Lemma 3.1 that there exists a constant $C > 0$ such that

$$|\chi - 1| \le C|h| \qquad \text{in } J_\varepsilon. \tag{3.13}$$

3.1.2. *Proof of Theorem 3.1.* Using the rescaling $x = \varepsilon y$ and the corresponding rescaled Fermi coordinate $(t_1, \dots, t_{N-1}, h) = \varepsilon(\tau_1, \dots, \tau_{N-1}, s)$, problem (3.3) can be written in $\varepsilon^{-1}J_\varepsilon$ as

$$\begin{aligned} &\Delta_{\varepsilon^{-2}g^T} u + \partial_{ss}^2 u + \varepsilon(s\tilde D^{(2)} + \tilde D^{(1)})u - u + u^2 = 0, \quad \text{in } \varepsilon^{-1}J_\varepsilon, \\ &-\partial_s u + \kappa u = a, \quad \text{on } \varepsilon^{-1}\Gamma, \end{aligned} \tag{3.14}$$

where $\tilde D^{(2)}$ and $\tilde D^{(1)}$ are, respectively, second and first order differential operators with bounded coefficients in $\varepsilon^{-1}J_\varepsilon$.

Using w_a given in (3.4) as a first approximation for a solution of (3.14) we calculate

$$\Delta_y w_a - w_a + w_a^2 = \varepsilon(s\tilde D^{(2)} + \tilde D^{(1)})w_a \le c\varepsilon(|s| + 1)e^{-s} \quad \text{for some constant } c > 0.$$

The boundary condition is obviously satisfied. Next we let $\eta(t)$ be a cut-off function such that $\eta(t) = 1$ for $t \le 1$ and $\eta(t) = 0$ for $t \ge 2$. Letting $\eta_\delta(t) = \eta(t/\delta)$ we find that

$$\tilde w_a = \eta_{-\frac{1}{2}(\gamma+1)\varepsilon \log \varepsilon}(s) w_a(s),$$

is a good approximation of problem (3.3).

Consider next the eigenvalue problem

$$-(\Delta_{\varepsilon^{-2}g^T}\phi + \partial_{ss}^2\phi - \phi + 2w_a\phi) = \mu\phi, \qquad -\partial_s\phi + \kappa\phi = 0, \tag{3.15}$$

and note that $-w_a'(s)$ is positive (since $y_a > y_c > 0$) and moreover it is also a super-solution of

$$-(\Delta_{\varepsilon^{-2}g^T}\phi + \partial_{ss}^2\phi - \phi + 2w_a\phi) = 0, \qquad -\partial_s\phi + \kappa\phi = 0.$$

and the eigenvalues, $\{\mu_j\}_{i\ge1}$, of (3.15) are therefore positive. Thus, for $\varepsilon > 0$ sufficiently small, the eigenvalues $\{\mu_j^\varepsilon\}_{i\ge1}$, of the eigenvalue problem problem

$$-(\Delta_y\phi - \phi + 2\tilde w_a\phi) = \mu\phi, \qquad -\partial_s\phi + \kappa\phi = 0, \tag{3.16}$$

on $H^1(\Omega_\varepsilon)$ are likewise positive and moreover they satisfy $\mu_j^\varepsilon \to \mu_j$ as $\varepsilon \to 0^+$ for all $j \geq 0$. In fact, if we denote the eigenvalues of $\Delta_{\partial\Omega}(= -\Delta_{g^T})$ by $0 < \mu_1^* < \mu_2^* \leq \ldots$, then $\mu_j^\varepsilon = \mu_j + \mu_j^* \varepsilon^2$ for all $j \geq 0$.

To obtain an exact solution of (3.14) we let $u_\varepsilon(y) = \tilde{w}_a + v_\varepsilon(y)$ and put it into the equation for u_ε with which we obtain the equation for v_ε

$$(\Delta_y - 1 + 2\tilde{w}_a)\, v_\varepsilon + E_\varepsilon + K_\varepsilon(v_\varepsilon) = 0, \quad \text{in } \Omega_\varepsilon, \tag{3.17a}$$

$$-\partial_s v_\varepsilon + \kappa v_\varepsilon = 0 \quad \text{on } \partial\Omega_\varepsilon, \tag{3.17b}$$

where

$$E_\varepsilon \equiv \Delta_y \tilde{w}_a - \tilde{w}_a + \tilde{w}_a^2, \qquad K_\varepsilon(v_\varepsilon) \equiv |\tilde{w}_a + v_\varepsilon|^2 - \tilde{w}_a^2 - 2\tilde{w}_a v_\varepsilon.$$

It is easy to estimate that

$$|E_\varepsilon| \leq c\varepsilon(1 + |s|)e^{-s}, \qquad |K_\varepsilon(v_\varepsilon)| \leq c|v_\varepsilon|^2.$$

Since $-(\Delta_y - 1 + 2\tilde{w}_a)$ is an increasing operator, by the Krein-Rutman theorem, the eigenfunction ϕ_1^ε corresponding to the principal eigenvalue μ_1^ε can be chosen positive in $\bar{\Omega}_\varepsilon$ and satisfying $\|\phi_1^\varepsilon\|_{L^\infty(\Omega_\varepsilon)} = 1$. By elliptic regularity we also have $|\phi_1^\varepsilon| \lesssim \exp(-c\varepsilon^{-1} d(x, \partial\Omega))$. Then we can choose $c_* > 0$ sufficiently large such that $c_*\varepsilon\phi_1^\varepsilon$ is a positive super-solution and $-c_*\varepsilon\phi_1^\varepsilon$ is a negative sub-solution of (3.17). Therefore the problem (3.17) has a solution v_ε and $u_\varepsilon = \tilde{w}_a + v_\varepsilon$ is a solution of (3.3). Moreover, by the maximum principle u_ε is positive. With $U_\varepsilon = \xi_\varepsilon u_\varepsilon$ equation (3.6) is established.

To complete the proof we use the expansion of the volume form (3.12) and (3.13) to obtain

$$\begin{aligned}\xi_\varepsilon &= \frac{1}{\varepsilon|\Omega|}\int_\Omega U_\varepsilon^2\, dx = \frac{\xi_\varepsilon^2}{\varepsilon|\Omega|}\int_\Omega w_a^2(h/\varepsilon)\chi \mathrm{d}\sigma\mathrm{d}h + \mathcal{O}(1)\xi_\varepsilon^2 \\ &= (1 + \mathcal{O}(\varepsilon))\frac{\xi_\varepsilon^2}{\varepsilon|\Omega|}\int_{J_\varepsilon} w_a^2(h/\varepsilon)\mathrm{d}\sigma\mathrm{d}h = (1 + \mathcal{O}(\varepsilon))\frac{\xi_\varepsilon^2|\partial\Omega|}{|\Omega|}\int_0^{\varepsilon^{\gamma-1}} w_a^2(s)\mathrm{d}s.\end{aligned}$$

The estimate (3.7) then follows from the facts that $\gamma - 1 < 0$ and that the function $w_a(s)$ decays exponentially as $s \to \infty$.

3.2. **The stability of the boundary layer solution.** In this section we prove that the boundary layer solution from the preceding section is linearly stable. Our main result is the following.

Theorem 3.2. *If $\tau \geq 0$ is sufficiently small then the boundary layer solution in Theorem 3.1 is linearly stable.*

Proof. Linearizing (3.1) at the solution $(U_\varepsilon, \xi_\varepsilon)$ in Theorem 3.1 yields the eigenvalue problem

$$\lambda_\varepsilon\phi_\varepsilon = \varepsilon^2\Delta\phi_\varepsilon - \phi_\varepsilon + \frac{2U_\varepsilon\phi_\varepsilon}{\xi_\varepsilon} - \frac{U_\varepsilon^2}{\xi_\varepsilon^2}\psi_\varepsilon, \tag{3.18}$$

$$\tau\lambda_\varepsilon\psi_\varepsilon = -\psi_\varepsilon + \frac{2}{\varepsilon|\Omega|}\int_\Omega U_\varepsilon\phi_\varepsilon, \tag{3.19}$$

with the boundary condition

$$\varepsilon\partial_\nu\phi_\varepsilon + \kappa\phi_\varepsilon = 0.$$

Assume to the contrary that (3.18) admits an eigenvalue λ_ε such that $\mathrm{Re}\lambda_\varepsilon \geq 0$ with corresponding eigenfunction ϕ_ε. By comparing with the principal eigenfunction ϕ_1^ε of $-(\Delta_y - 1 + 2\tilde{w}_a)$ (see above) we get $|\phi_\varepsilon| \lesssim \exp(-c\frac{d(x,\partial\Omega)}{\varepsilon})$.

Using the Fermi coordinates, we write $\phi_\varepsilon = \phi_\varepsilon(x', h)$ and $U_\varepsilon = U_\varepsilon(x', h)$, where $x' \in \partial\Omega$ and $h \in [0, \varepsilon^\gamma)$, as in (3.10). Letting

$$\tilde{\phi}_\varepsilon(x', s) = \phi_\varepsilon(x', \varepsilon s), \quad \tilde{U}_\varepsilon(x', s) = U_\varepsilon(x', \varepsilon s),$$

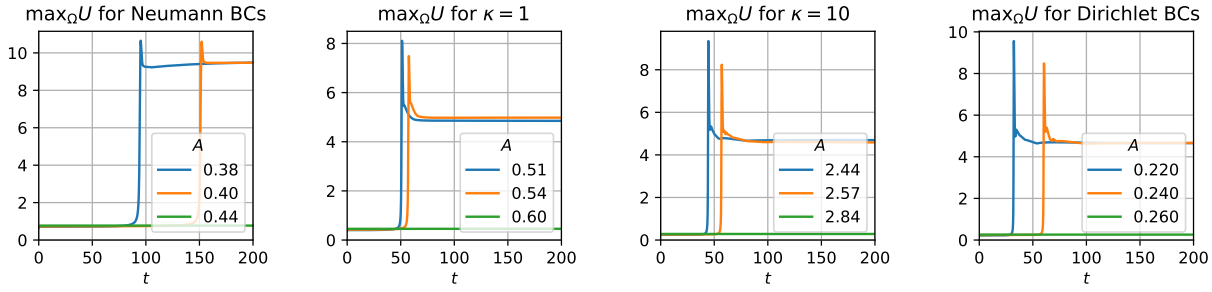

(A) (B) (C) (D)

FIGURE 8. Plots of $\max_{x\in\Omega} U(x,t)$ versus $t>0$ for selected values of A obtained by numerically solving (3.18) with $\varepsilon = 0.05$ and $\tau = 0.2$ and with (A) Neumann BCs, mixed BCs with (B) $\kappa = 1$ and (C) $\kappa = 10$, and (D) Dirichlet BCs. In each case (3.6) and (3.7) were used as the initial conditions.

and using the profile of $(U_\varepsilon, \xi_\varepsilon)$ we may assume that $\tilde{U}_\varepsilon(x',s) \to \xi_\varepsilon w_a(s)$ and $\tilde{\phi}_\varepsilon(x',s) \to \tilde{\phi}(x',s)$ in $H^2(\partial\Omega\times[0,+\infty)) \cap C^2_{loc}(\partial\Omega\times[0,+\infty))$ as $\varepsilon\to 0$. Then

$$\int_\Omega U_\varepsilon \phi_\varepsilon \, dx \sim \xi_\varepsilon \varepsilon \int_0^\infty w_a(s) \int_{\partial\Omega} \tilde{\phi}(x',s) d\sigma ds$$

and therefore

$$\psi_\varepsilon \sim \frac{1}{1+\tau\lambda_\varepsilon} \frac{2}{|\partial\Omega|} \frac{\int_0^\infty w_a(s) \int_{\partial\Omega} \tilde{\phi}(x',s) d\sigma ds}{\int_0^\infty w_a^2(s) ds}$$

Since $\tau \geq 0$ and $\mathrm{Re}\lambda_\varepsilon > 0$ the boundedness of ϕ_ε and hence also of $\tilde{\phi}$ implies that the eigenvalues λ_ε are bounded and we may assume further that $\lambda_\varepsilon \to \lambda$ locally in $\mathbb{C}$. Using the profile of the functions $(U_\varepsilon, \xi_\varepsilon)$ we deduce from (3.18) that for small $\varepsilon > 0$

$$\lambda\tilde{\phi} \sim \partial^2_{ss}\tilde{\phi} + \varepsilon^2 \Delta_{\partial\Omega}\tilde{\phi} - \tilde{\phi} + 2w_a\tilde{\phi} - \frac{1}{1+\tau\lambda} \frac{2}{|\partial\Omega|} \frac{\int_0^\infty w_a(s) \int_{\partial\Omega} \tilde{\phi}(x',s) d\sigma ds}{\int_0^\infty w_a^2(s) ds} w_a^2, \tag{3.20}$$

and integrating over $\partial\Omega$ we arrive at the following equation for $\phi_1(s) = \int_{\partial\Omega} \tilde{\phi}(x',s) d\sigma$

$$\lambda\phi_1 = \partial^2_{ss}\phi_1 - \phi_1 + 2w_a\phi_1 - \frac{2}{1+\tau\lambda} \frac{\int_0^\infty w_a(s)\phi_1(s) ds}{\int_0^\infty w_a^2(s) ds} w_a^2. \tag{3.21}$$

By the results in Section 2.3 and in particular Theorem 2.2 we deduce that for $\tau \geq 0$ sufficiently small if $\mathrm{Re}(\lambda) \geq 0$ then $\phi_1(s) \equiv 0$. Therefore we assume that $\int_{\partial\Omega} \tilde{\phi}(x',s) d\sigma \equiv 0$ so that the relevant eigenvalue problem is

$$\lambda\tilde{\phi} = \partial^2_{ss}\tilde{\phi} + \varepsilon^2 \Delta_{\partial\Omega}\tilde{\phi} - \tilde{\phi} + 2w_a\tilde{\phi}, \tag{3.22a}$$

together with the boundary condition

$$-\partial_s\tilde{\phi} + \kappa\tilde{\phi} = 0 \ \text{ for } \ s = 0. \tag{3.22b}$$

Since the shift parameter exceeds the critical value $y_c(\kappa)$, by Lemma 2.1 the principal eigenfunction Φ_0 of the one-dimensional linearized operator $\partial^2_{ss} - 1 + 2w_a$ is of one sign and the corresponding principal eigenvalue satisfies $\Lambda_0 < 0$. In particular choosing Φ_0 to be strictly positive and multiplying it by an appropriate cut-off function we obtain a super-solution to the higher-dimensional problem (3.22) from which we deduce the contradiction $\mathrm{Re}\lambda \leq \Lambda_0 < 0$.

□

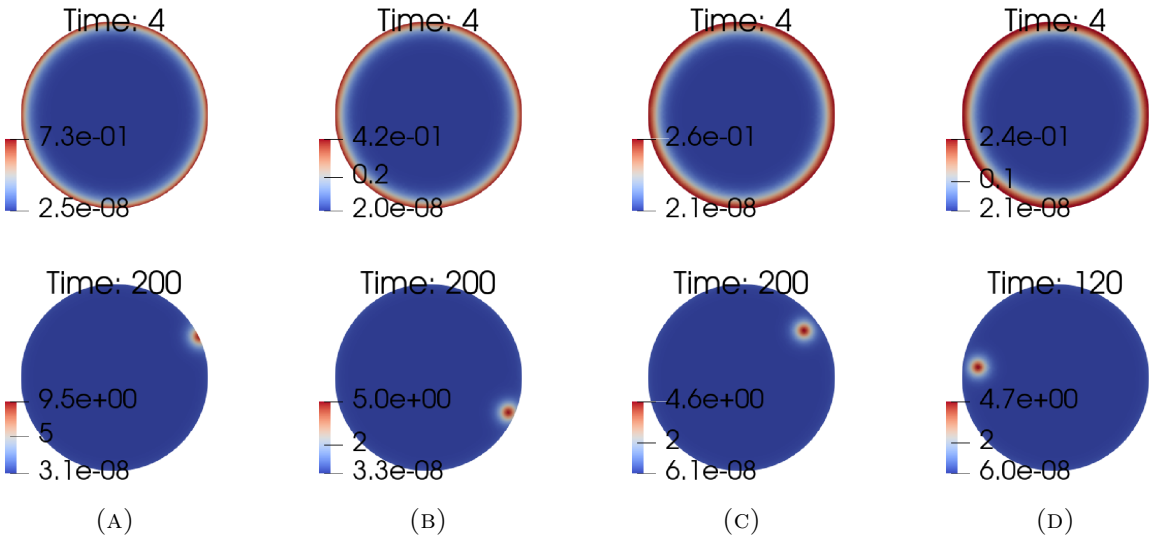

FIGURE 9. Plots of the rescaled solution $\varepsilon U(x,t)$ to (3.18) at selected times $t>0$ with $A=0.95A_{\min}$ and (A) Neumann BCs, mixed BCs with (B) $\kappa=1$ and (C) $\kappa=10$, and (D) Dirichlet BCs. Remaining parameters used are $\tau=0.5$ and $\varepsilon=0.05$.

3.3. **Numerical Simulations.** To illustrate Theorems 3.1 and 3.2 above we use FlexPDE 6 [20] to numerically solve (3.18) with $\tau=0.5$ and $\varepsilon=0.05$ for different choices of BCs obtained by varying κ and A. For each simulation we use (3.6) and (3.7) as initial conditions. In Figure 8 we plot $\max_{x\in\Omega}U(x,t)$ versus $t>0$ for mixed BCs with $\kappa=0,1,10$ as well as with Dirichlet BCs. For each choice of BCs we select three values of A corresponding to 90%, 95%, and 105% of the minimum value $A_{\min}$ given by (3.5) and (3.9) for mixed and Dirichlet BCs respectively. In each case our numerical simulations support the results of Theorem 3.2 that the boundary layer solution is linearly stable for $A>A_{\min}$. Moreover, for values of $A<A_{\min}$ we observe that the boundary layer solution is linearly unstable. Interestingly, as illustrated in Figure 9, we observe that when $A<A_{\min}$ the unstable boundary layer tends to a solution consisting of a small boundary layer together with a near boundary spike. The detailed study of this boundary layer and near-boundary spike solution is beyond the scope of this paper and will be addressed in a future study.

4. CONCLUSION

We have used a combination of asymptotic and rigorous methods as well as numerical simulations to study the structure and linear stability of boundary-layer type localized solutions to the singularly perturbed Gierer-Meinhardt system in multi-dimensional domains. In the case of a one-dimensional domain we used the method of matched asymptotic expansions to reduce the construction of multi-spike solutions to that of solving a nonlinear algebraic system for the spike heights and their locations. This method has been extensively used in the context of singularly perturbed reaction-diffusion systems and our primary contribution here is the extension to the case where the slowly diffusing activator has inhomogeneous Neumann, mixed, or Dirichlet boundary conditions. Our results in this direction can be seen as an extension of those obtained for inhomogeneous Neumann boundary conditions in [7] and homogeneous mixed boundary conditions in [17]. In particular we found that the shift-parameter continues to play a critical role in the stability of a single spike solution, and furthermore we found that for each of the boundary conditions considered the resulting two-spike solutions share many qualitative similarities. Specifically, the stability

of an asymmetric solution for certain parameter regimes was observed for all choices of boundary conditions.

When the GM model is posed on a connected and bounded domain with smooth boundary in two and higher dimensions we restricted our attention to the shadow limit in which the inhibitor diffusivity is taken to be infinitely large. In this limit we provided a rigorous treatment of both the existence and stability of a boundary layer solution when the value of the inhomogeneity at the boundary exceeds a critical value. Specifically we proved that when $A > A_{\min}(\kappa)$ as in (3.5) and (3.9) for mixed and Dirichlet BCs respectively, then a boundary-layer solution obtained by extending a one-dimensional spike along the boundary of the domain both exists and is linearly stable. The asymptotic expression given for this boundary layer in Theorem 3.1 can be formally used when $A < A_{\min}(\kappa)$ though our proofs, which rely crucially on the stability of the linearized operator, are no longer valid in this regime. However we anticipate that when $A < A_{\min}(\kappa)$ such a boundary layer solution is unstable and this prediction is supported in our numerical simulations.

We conclude with some suggestions for future research. First, the rigorous stability analysis for the single-spike solution performed in §2.3 used a continuation argument which provides stability properties for a limited range of y_0 and μ values. An open problem is to extend these regions to provide a complete characterization of the linear stability of the single spike solution, and in particular to prove the conjecture that the single spike solution is stable for all $\mu > \max(\mu_c(y_0, \kappa), 0)$ for all $y_{\min} < y_0 < \infty$. In the case of a higher dimensional domain it would be worthwhile to perform a detailed analysis, either formal or rigorous, of localized solutions that arise when $A < A_{\min}$. It would be particularly interesting to provide a detailed analysis of the solution consisting of both a boundary layer and a near-boundary spike that was observed in our numerical simulations in Figure 9. One question to ask is whether a similar situation to the one-dimensional case, where both a symmetric and asymmetric solution can be stable for certain parameter values, arises in higher dimensions. In addition to being mathematically interesting we also anticipate that such solutions will play an important role in singularly perturbed problems incorporating bulk-surface coupling [5] and will also provide insights into the phenomena of isolated patterns [14].

Acknowledgements

D. Gomez is supported by NSERC of Canada and the Simons Foundation. L. Mei is supported by the National Natural Science Foundation of China: grant no. 11771125 J. Wei is partially supported by NSERC of Canada.

References

[1] H. Berestycki and J. Wei. On singular perturbation problems with robin boundary condition. *Annali della Scuola Normale Superiore di Pisa-Classe di Scienze*, 2(1):199–230, 2003.

[2] R. Dillon, P. Maini, and H. Othmer. Pattern formation in generalized turing systems. i: Steady-state patterns in systems with mixed boundary conditions. *Journal of Mathematical Biology*, 32, 04 1994.

[3] A. Doelman, R. A. Gardner, and T. Kaper. Large stable pulse solutions in reaction-diffusion equations. *Indiana U. Math. Journ.*, 50(1):443–507, 2001.

[4] A. Gierer and H. Meinhardt. A theory of biological pattern formation. *Kybernetik*, 12(1):30–39, Dec 1972.

[5] D. Gomez, M. J. Ward, and J. Wei. The linear stability of symmetric spike patterns for a bulk-membrane coupled Gierer-Meinhardt model. *SIAM J. Appl. Dyn. Syst.*, 18(2):729–768, 2019.

[6] D. Gomez, M. J. Ward, and J. Wei. An asymptotic analysis of localized 3-d spot patterns for gierer-meinhardt model: Existence, linear stability and slow dynamics. *arXiv preprint arXiv:2008.04535*, 2020.

[7] D. Gomez and J. Wei. Multi-spike patterns in the gierer–meinhardt system with a nonzero activator boundary flux. *Journal of Nonlinear Science*, 31(2):37, Mar 2021.

[8] C. Gui and J. Wei. Multiple interior peak solutions for some singularly perturbed Neumann problems. *J. Differential Equations*, 158(1):1–27, 1999.

[9] J. Halatek, F. Brauns, and E. Frey. Self-organization principles of intracellular pattern formation. *Philosophical Transactions of the Royal Society B: Biological Sciences*, 373(1747):20170107, 2018.

[10] J. Halatek and E. Frey. Highly canalized mind transfer and mine sequestration explain the origin of robust mincde-protein dynamics. *Cell reports*, 1:741–52, 06 2012.
[11] D. Iron, M. J. Ward, and J. Wei. The stability of spike solutions to the one-dimensional Gierer-Meinhardt model. *Phys. D*, 150(1-2):25–62, 2001.
[12] M. Kowalczyk. Multiple spike layers in the shadow Gierer-Meinhardt system: existence of equilibria and the quasi-invariant manifold. *Duke Math. J.*, 98(1):59–111, 1999.
[13] A. L. Krause, V. Klika, J. Halatek, P. K. Grant, T. E. Woolley, N. Dalchau, and E. A. Gaffney. Turing patterning in stratified domains. *Bulletin of Mathematical Biology*, 82(10):1–37, 2020.
[14] A. L. Krause, V. Klika, P. K. Maini, D. Headon, and E. A. Gaffney. Isolating patterns in open reaction-diffusion systems. *arXiv preprint arXiv:2009.13114*, 2020.
[15] H. Levine and W.-J. Rappel. Membrane-bound Turing patterns. *Phys. Rev. E (3)*, 72(6):061912, 5, 2005.
[16] A. Madzvamuse, A. H. W. Chung, and C. Venkataraman. Stability analysis and simulations of coupled bulk-surface reaction-diffusion systems. *Proc. A.*, 471(2175):20140546, 18, 2015.
[17] P. K. Maini, J. Wei, and M. Winter. Stability of spikes in the shadow gierer-meinhardt system with robin boundary conditions. *Chaos: An Interdisciplinary Journal of Nonlinear Science*, 17(3):037106, 2007.
[18] A. Malchiodi and M. Montenegro. Boundary concentration phenomena for a singularly perturbed elliptic problem. *Communications on Pure and Applied Mathematics*, 55(12):1507–1568, 2002.
[19] F. Pacard, F. Pacella, and B. Sciunzi. Solutions of semilinear elliptic equations in tubes. *Journal of Geometric Analysis*, 24(1):445–471, Jan 2014.
[20] PDE Solutions Inc. *FlexPDE 6*. URL: http://www.pdesolutions.com.
[21] A. Rätz and M. Röger. Turing instabilities in a mathematical model for signaling networks. *J. Math. Biol.*, 65(6-7):1215–1244, 2012.
[22] I. Takagi. Point-condensation for a reaction-diffusion system. *J. Differential Equations*, 61(2):208–249, 1986.
[23] A. M. Turing. The chemical basis of morphogenesis. *Philos. Trans. Roy. Soc. London Ser. B*, 237(641):37–72, 1952.
[24] J. C. Tzou and M. J. Ward. The stability and slow dynamics of spot patterns in the 2D Brusselator model: the effect of open systems and heterogeneities. *Phys. D*, 373:13–37, 2018.
[25] M. J. Ward and J. Wei. Asymmetric spike patterns for the one-dimensional Gierer-Meinhardt model: equilibria and stability. *European J. Appl. Math.*, 13(3):283–320, 2002.
[26] M. J. Ward and J. Wei. Hopf bifurcation of spike solutions for the shadow Gierer-Meinhardt model. *European J. Appl. Math.*, 14(6):677–711, 2003.
[27] J. Wei. On single interior spike solutions of the Gierer-Meinhardt system: uniqueness and spectrum estimates. *European J. Appl. Math.*, 10(4):353–378, 1999.
[28] J. Wei and M. Winter. Spikes for the Gierer-Meinhardt system in two dimensions: the strong coupling case. *J. Differential Equations*, 178(2):478–518, 2002.
[29] J. Wei and M. Winter. Existence, classification and stability analysis of multiple-peaked solutions for the Gierer-Meinhardt system in $\mathbf{R}^1$. *Methods Appl. Anal.*, 14(2):119–163, 2007.
[30] J. Wei and M. Winter. *Mathematial aspects of pattern formation in biological systems*, volume 189. Applied Mathematical Sciences Series, Springer, 2014.
[31] J. Wei and L. Zhang. On a nonlocal eigenvalue problem. *Annali della Scuola Normale Superiore di Pisa - Classe di Scienze*, Ser. 4, 30(1):41–61, 2001.